

Extratropical transition of tropical cyclones in a multiresolution ensemble of atmosphere-only and fully coupled global climate models

Article

Accepted Version

Baker, A. J. ORCID: <https://orcid.org/0000-0003-2697-1350>, Roberts, M. J., Vidale, P. L. ORCID: <https://orcid.org/0000-0002-1800-8460>, Hodges, K. I. ORCID: <https://orcid.org/0000-0003-0894-229X>, Seddon, J., Vanniere, B. ORCID: <https://orcid.org/0000-0001-8600-400X>, Haarsma, R. J., Schiemann, R. ORCID: <https://orcid.org/0000-0003-3095-9856>, Kapetanakis, D., Tourigny, E., Lohmann, K., Roberts, C. D. and Terray, L. (2022) Extratropical transition of tropical cyclones in a multiresolution ensemble of atmosphere-only and fully coupled global climate models. *Journal of Climate*, 35 (16). pp. 5283-5306. ISSN 1520-0442 doi: 10.1175/JCLI-D-21-0801.1 Available at <https://centaur.reading.ac.uk/105122/>

It is advisable to refer to the publisher's version if you intend to cite from the work. See [Guidance on citing](#).

Published version at: <https://journals.ametsoc.org/view/journals/clim/aop/JCLI-D-21-0801.1/JCLI-D-21-0801.1.xml>

To link to this article DOI: <http://dx.doi.org/10.1175/JCLI-D-21-0801.1>

Publisher: American Meteorological Society

All outputs in CentAUR are protected by Intellectual Property Rights law, including copyright law. Copyright and IPR is retained by the creators or other copyright holders. Terms and conditions for use of this material are defined in the [End User Agreement](#).

www.reading.ac.uk/centaur

CentAUR

Central Archive at the University of Reading

Reading's research outputs online

Extratropical transition of tropical cyclones in a multiresolution ensemble of atmosphere-only and fully coupled global climate models

Alexander J. Baker^{1,*}, Malcolm J. Roberts², Pier Luigi Vidale¹, Kevin I. Hodges¹, Jon Seddon², Benoît Vannière¹, Rein J. Haarsma³, Reinhard Schiemann¹, Dimitris Kapetanakis³, Etienne Tourigny⁴, Katja Lohmann⁵, Christopher D. Roberts⁶, and Laurent Terray⁷

¹ National Centre for Atmospheric Science and Department of Meteorology, University of Reading, Reading, Berkshire, UK

² Met Office Hadley Centre, Exeter, Devon, UK

³ Koninklijk Nederlands Meteorologisch Instituut, De Bilt, The Netherlands

⁴ Earth Sciences Department, Barcelona Supercomputing Center, Barcelona, Spain

⁵ Max Planck Institut für Meteorologie, Hamburg, Germany

⁶ European Centre for Medium-Range Weather Forecasts (ECMWF), Reading, UK

⁷ Climat, Environnement, Couplages et Incertitudes, Centre Européen de Recherche et de Formation Avancée en Calcul Scientifique (CERFACS), Toulouse, France

* alexander.baker@reading.ac.uk

For submission to *Journal of Climate*

Corresponding author: Dr Alexander J. Baker

National Centre for Atmospheric Science

Department of Meteorology,

University of Reading

Earley Gate, Whiteknights Road, Reading, Berkshire RG6 6ES, UK

+44 (0) 118 377 762

Abstract

Tropical cyclones undergo extratropical transition (ET) in every ocean basin. Projected changes in ET frequency under climate change are uncertain and differ between basins, so multimodel studies are required to establish confidence. We used a feature-tracking algorithm to identify tropical cyclones and performed cyclone phase-space analysis to identify ET in an ensemble of atmosphere-only and fully coupled global model simulations, run at various resolutions under historical (1950–2014) and future (2015–2050) forcing. Historical simulations were evaluated against five reanalyses for 1979–2018. Considering ET globally, ensemble-mean biases in track and genesis densities are reduced in the North Atlantic and Western North Pacific when horizontal resolution is increased from ~100 to ~25km. At high resolution, multireanalysis-mean climatological ET frequencies across most ocean basins as well as basins' seasonal cycles are reproduced better than in low-resolution models. Skill in simulating historical ET interannual variability in the North Atlantic and Western North Pacific is ~0.3, which is lower than for all tropical cyclones. Models project an increase in ET frequency in the North Atlantic and a decrease in the Western North Pacific. We explain these opposing responses by secular change in ET seasonality and an increase in lower-tropospheric, pre-ET warm-core strength, both of which are largely unique to the North Atlantic. Multimodel consensus about climate-change responses is clearer for frequency metrics than for intensity metrics. These results help clarify the role of model resolution in simulating ET and help quantify uncertainty surrounding ET in a warming climate.

1. Introduction

The impacts of tropical cyclones are not confined to the tropics. Their post-tropical evolution makes these storms an important natural hazard across the midlatitudes (Baker et al., 2021; Bieli et al., 2019; Evans et al., 2017; Jones et al., 2003; Keller et al., 2019). The poleward propagation of tropical cyclones and the occurrence of extratropical transition (ET) exposes populous regions where risks to life and infrastructure are high—Northeast United States, maritime and eastern Canada, Western Europe, and East Asia—to hurricane-force wind speeds and extreme precipitation (Evans et al., 2017). In the North Atlantic, tropical-origin systems reached Northeast North America and Europe almost every year since 1979 (Baker et al., 2021), including recent intense landfalls. For instance, Hurricane Sandy (22nd–29th October, 2012)—the fourth costliest (by inflation-adjusted losses) North Atlantic hurricane yet recorded (Weinkle et al., 2018)—caused devastation across the Northeast United States and eastern Canada (Blake et al., 2013). Ex-hurricane Ophelia (9th–15th October, 2017) led to loss of life and severe wind damage across Ireland, the United Kingdom, and Scandinavia (Rantanen et al., 2020; Stewart, 2018). At midlatitude landfall, both systems were post-tropical, having begun ET, but possessed hurricane-like intensities, the human and economic impacts of which were felt across substantial areas. In the Western North Pacific, Typhoon Nabi (29th August–12th September, 2005) impacted two thirds of Japan’s prefectures as both a tropical and transitioning cyclone before undergoing cyclolysis over Alaska (Harr et al., 2008). These events, along with the current lack of consensus regarding ET in a changing climate, heighten the urgency with which global studies of historical and near-future post-tropical cyclone activity are needed.

Tropical cyclones undergo ET in every ocean basin (Hart and Evans, 2001; Studholme et al., 2015; Wood and Ritchie, 2014; Zarzycki et al., 2017), but pronounced interannual variability (Baker et al., 2021) and basin-to-basin differences (Bieli et al., 2019) exist. Transitioning cyclones are also known to influence the large-scale circulation, such as Hurricane Debbie in 1982 (Laurila et al., 2019), and excite or amplify downstream Rossby waves (Evans et al., 2017; Jones et al., 2003; Keller et al., 2019; Michaelis and Lackmann, 2019). These cyclone-wave interactions influence downstream weather (Grams and Blumer, 2015; Keller et al., 2019). Of those cyclones which undergo ET, an appreciable proportion reintensify under favourable environmental conditions, where appropriate phasing between the transitioning cyclone and the upper-tropospheric flow pattern enhances baroclinic instability (Keller et al.,

2019). During and after ET, baroclinicity (Evans et al., 2017) and diabatic heating (Rantanen et al., 2020) may reintensify the post-tropical cyclone.

Over the period of 1979–2018, statistically significant positive trends in the frequency of North Atlantic ET events exist in several, but not all, reanalysis datasets (Baker et al., 2021). Existing climate model projections underline the plausibility of increased tropical and post-tropical cyclone activity in the midlatitudes in response to anthropogenic warming. There is evidence that more frequent ET events may occur in the future in the North Atlantic (Baatsen et al., 2015; Haarsma et al., 2013; Liu et al., 2017; Michaelis and Lackmann, 2019) and Western North Pacific (Bieli et al., 2020) ocean basins, but no consensus yet exists across studies, modelling campaigns, and methodologies. Moreover, best-track data limitations, which are well documented (Chang and Guo, 2007; Delgado et al., 2018; Hagen et al., 2012; Vecchi and Knutson, 2008), engender substantial uncertainty in observed trends (Lanzante, 2019; Moon et al., 2019). Additionally, natural, multidecadal variability in tropical-cyclone frequency is yet to be accounted for (Knutson et al., 2020). Although global climate models project reduced frequencies of tropical cyclones, more intense tropical cyclones are expected in response to twenty-first-century warming (Knutson et al., 2020), potentially allowing a higher proportion of cyclones to survive cooler midlatitude sea-surface temperatures experienced prior to and during ET (Michaelis and Lackmann, 2019). Other factors, particularly changes in shear, will also be important, with current evidence suggesting that these will undergo ET-favourable future changes (Jung and Lackmann, 2021; Liu et al., 2017; Michaelis and Lackmann, 2021). Increased future ET event frequency is also consistent with the projected expansion of tropical-cyclone genesis regions (Studholme et al., 2022), potentially reducing the mean displacement cyclones must undergo prior to midlatitude ET. Together, these changes imply an increase in post-tropical cyclone impacts across populated midlatitude regions, and idealised experiments suggest an increase in ET-related, high-impact weather across Europe (Jung and Lackmann, 2021), where our understanding of historical risks is developing (Baker et al., 2021). Studies of historical and future model simulations are therefore needed to assess both contemporary risk and future changes more comprehensively.

One aspect of climate model evaluation important for both tropical and extratropical cyclones is understanding the role of horizontal resolution in simulated climates, prompted by recent developments in high-performance computing and data-management facilities. With

increases in model resolution to approximately 25 km, improved fidelity is anticipated for many synoptic phenomena, particularly tropical and midlatitude cyclones, which ultimately feed back onto the large scale. Recent studies have now firmly established that increasing model resolution improves simulated tropical-cyclone frequency statistics across most ocean basins (Manganello et al., 2019; Roberts et al., 2020a), leads to a more realistic global spatial distribution (Roberts et al., 2020a; Roberts et al., 2015; Strachan et al., 2013), and results in more realistic simulated warm-core vertical structures (Vannière et al., 2020). Moreover, model resolution is a key constraint on the intensity which simulated cyclones may reach (Davis, 2018). It is anticipated that atmospheric resolutions of ~ 50 km or finer ($\sim 0.25^\circ$ ocean-model resolution) will yield improvement in the simulation of post-tropical cyclones and ET (Haarsma, 2021). However, no systematic multimodel studies of ET have been undertaken, and the impact of increasing model resolution (atmosphere and ocean) on simulated ET is also yet to be quantified. We address these issues in this paper using model simulations from the 6th phase of the Coupled Model Intercomparison Project (CMIP6), which follow an experimental protocol designed to isolate the impacts of changes in model resolution.

In this study of the representation of tropical cyclones undergoing ET across a multimodel ensemble, we focus on climatological statistics, interannual variability, and cyclone structure and intensity. These analyses are centred around two questions. What is the impact of increasing model atmospheric resolution on simulated ET? What changes in ET metrics under climate change are consistent across models? This paper continues in section 2 with a description of the model and reanalysis data as well as the cyclone-tracking and analysis methodologies. Our results are presented in section 3 and our conclusions are summarised, with further discussion, in section 4.

2. Data and methodology

2.1 Reanalysis data

Tropical cyclone best-track datasets are not well suited to analysis of cyclones undergoing ET because there are known heterogeneities within individual datasets (Barcikowska et al., 2012; Chu et al., 2002; Kossin et al., 2007; Vecchi and Knutson, 2008, 2011), especially for storms' post-tropical stages, under-counting biases (Chang and Guo, 2007; Delgado et al., 2018; Hagen et al., 2012), and differences between operational centres' data-collection

methodologies (Hodges et al., 2017; Schreck III et al., 2014). We therefore evaluated model simulations against five global reanalyses (Table 1): the European Centre for Medium-Range Weather Forecasts' Interim Reanalysis (ERA-Interim; Dee et al., 2011) and Fifth Reanalysis (ERA5; Hersbach et al., 2020); the Japanese 55-year Reanalysis (JRA55; Kobayashi et al., 2015); the National Aeronautics and Space Administration's Modern-Era Retrospective Analysis for Research and Applications version 2 (MERRA2; Molod et al., 2015); and the combined National Centers for Environmental Prediction Climate Forecast System Reanalysis and Climate Forecast System version 2 dataset (NCEP; Saha et al., 2014)—the sole fully coupled (atmosphere, ocean, land surface, and sea ice) reanalysis used herein. Between reanalyses, differing forecast model formulations and resolutions (horizontal and vertical), as well as data-assimilation schemes lead to differences in the representation of tropical-cyclone vertical structure, which was examined by Hodges et al. (2017). Baker et al. (2021) found that interannual variability in the number ET events is well correlated between reanalyses, but the percentage of tropical cyclones undergoing ET agrees less well between reanalyses on the interannual timescale. It is therefore necessary to consider multiple reanalyses as an observation-based reference, against which models may be evaluated.

| Reanalysis | Analysis period | Analysis grid | Model resolution (grid spacing) | Data assimilation | Sample sizes (n_{NH} , n_{SH}) |
|------------|-----------------|---------------|------------------------------------|------------------------|---|
| ERA5 | 1979–2017 | 512x256 | TL255L60 (80 km) | 4D-Var. | 35.4, 37.0 |
| ERA5 | 1979–2018 | 1140x721 | T639L137 (33km) | 4D-Var. | 35.4, 37.0 |
| JRA55 | 1959–2017 | 288x145 | TL319L60 (55 km) | 4D-Var. | 35.4, 37.0 |
| MERRA2 | 1980–2016 | 576x361 | Cubed sphere (50 km) | 3D-Var. + GSI + IAU | 35.4, 37.0 |
| NCEP | 1979–2016 | 720x361 | T382L64 (38 km) | 3D-Var. + GSI | 35.4, 37.0 |

Table 1. Reanalyses. Atmospheric mesh spacing at 50 °N in units of km is given in brackets.
3(4)D-Var.: 3(4)D variational data assimilation; GSI: Grid-point Statistical Interpolation;
IAU: Incremental Analysis Update. The representation of tropical and post-tropical cyclones
in these reanalyses were evaluated by Hodges et al. (2017) and (Baker et al., 2021),
respectively. Annual-mean global sample sizes (cyclones year⁻¹) for all tropical cyclones
undergoing ET for each reanalysis are given as n_{NH} , n_{SH} .

2.2 The multiresolution PRIMAVERA model ensemble

We evaluated CMIP6 High-Resolution Model Intercomparison Project (HighResMIP; Haarsma et al., 2016) historical and future atmosphere-only (Tier 1 and Tier 3, respectively), including interaction with the land surface, and fully coupled (Tier 2) simulations from five global climate models (Table 2): CNRM-CM6.1 (Voldoire et al., 2019), EC-Earth3P (Haarsma et al., 2020), ECMWF-IFS (cycle 43r1; Roberts et al., 2018), HadGEM3-GC3.1 (Roberts et al., 2019; Williams et al., 2018), and MPI-ESM1.2 (Gutjahr et al., 2019). Each model participated in the European Commission Horizon2020-funded project PRIMAVERA (PProcess-based climate sIMulation: AdVances in high-resolution modelling and European climate Risk Assessments; primavera-h2020.eu). Historical (1950–2014) and future (2015–2050) atmosphere-only experiments are termed *highresSST-present* and *highresSST-future*, respectively, and fully coupled experiments are termed *hist-1950* and *highres-future*, respectively. Historical *highresSST-present* simulations were forced by HadISST2 daily sea-surface temperature (SST) at a resolution of 0.25° interpolated to each model's grid (no ocean mixed-layer model). Out to 2050, *highresSST-future* simulations were forced according to Representative Concentration Pathway 8.5 (RCP8.5). (Use of RCP8.5 allowed modelling centres to begin their model simulations before Shared Socioeconomic Pathways scenarios became available.) In HighResMIP, future simulations were performed with all models except ECMWF-IFS. The rate of projected sea-surface temperature (SST) warming was derived from an ensemble mean of CMIP5, with interannual variability derived from the historical period 1950–2014 (Haarsma et al., 2016).

Under the HighResMIP experimental protocol, minimal changes in model-tuning parameters were made between low- and high-resolution integrations to ensure that resolution-sensitivity studies were not confounded by substantial differences in model configurations between resolutions (Haarsma et al., 2016). Between low- and high-resolution configurations, no model-physics changes were made to the atmospheric components of CNRM-CM6.1 and EC-Earth3P, but minor adjustments were made to a single parameter in ECMWF-IFS (related to net surface energy balance), HadGEM3-GC3.1 (related to quasi-biennial oscillation period), and MPI-ESM1.2 (related to numerical stability). For the ocean model in coupled configurations, one key difference is the effects of mesoscale eddies are parameterised at low resolution ($\sim 1^\circ$) but partially resolved at high resolution ($\sim 0.25^\circ$) (e.g., Roberts et al., 2018; Roberts et al., 2019). For all models, shorter dynamical timesteps were used in the high-resolution integrations to ensure numerical stability. The effective resolutions of the high-

resolution model configurations, measured by kinetic energy spectra, resolve synoptic-scale dynamics (Klaver et al., 2020). Since this study concerns cyclone translation from the tropics to the extratropics, resolutions are given as a model's regular mesh spacing at a latitude of 50° (Table 2). For convenience, we refer to resolutions nominally (i.e., 'low' or 'high') as well as quantitatively, where necessary. A single ensemble member was analysed at each resolution for both the atmosphere-only and fully coupled experiments.

| Atmospheric model | Ocean model | Atmospheric dynamical core | Resolution nomenclature | Atmospheric resolution | Atmospheric mesh spacing |
|------------------------------|------------------------|---|------------------------------------|-----------------------------------|-------------------------------------|
| ARPEGE6.3 | NEMO | Spectral (linear, reduced Gaussian) | LR; HR | TL127; TL359 | 142; 50 km |
| IFS cyc36r4 | NEMO | Spectral (linear, reduced Gaussian) | LR; HR | TL255; TL511 | 71; 36 km |
| IFS cyc43r1 | NEMO3.4 | Spectral (cubic octahedral; reduced Gaussian) | LR; HR | Tco199; Tco399 | 50; 25 km |
| MetUM | NEMO | Grid point (SISL) | LM (LL); MM; HM (HH) | N96; N216; N512 | 135; 60; 25 km |
| ECHAM6.3 | MPIOM1.63 | Spectral (triangular; Gaussian) | HR; XR | T127; T255 | 67; 34 km |

| Model name | CNRM-CM6.1 | EC-Earth3P | ECMWF-IFS | HadGEM3-GC3.1 | MPI-ESM1.2 |
|------------|------------|------------|-----------|---------------|------------|
|------------|------------|------------|-----------|---------------|------------|

Table 2. The PRIMAVERA (HighResMIP) model ensemble. NEMO: Nucleus for European Modelling of the Ocean. MPIOM: Max Plank Institute Ocean Model. SISL: semi-implicit, semi-Lagrangian. For fully coupled simulations, the LL and HH configurations of HadGEM3-GC3.1 were also included; LL denoting low-resolution atmosphere and low-resolution (1 °) ocean and HH denoting high-resolution atmosphere and high-resolution (1/12 °) ocean. Atmosphere mesh spacing is given for 50 °N. Sample sizes for all tropical cyclones undergoing ET across this ensemble are given in Table 3. DOIs for each simulation are listed at primavera-h2020.eu/modelling/.

2.3 Lagrangian tropical-cyclone tracking

To identify and track the evolution of tropical cyclones, we used the objective feature-tracking algorithm—TRACK—of Hodges (1995), a well-established tool for identifying cyclones in reanalyses (Hodges et al., 2017) and model simulations (Roberts et al., 2020a). The TRACK algorithm was applied to six-hourly relative vorticity, computed from the zonal and meridional wind fields, which was vertically averaged over the 850-, 700- and 600-hPa levels and spectrally filtered. (Upper-level vorticity is used in subsequent identification.) Filtering to the T5–T63 spectral band removes both large, planetary scales (total wavenumbers 0–5) and small-scale noise (total wavenumbers >63). Vorticity maxima exceeding $0.5 \times 10^{-5} \text{ s}^{-1}$ (in the Northern Hemisphere; scaled by -1 in the Southern Hemisphere) were identified, initialised into tracks using a nearest-neighbour approach, and subsequently refined by minimising a cost function for track smoothness, subject to adaptive constraints on track displacement and smoothness (Hodges, 1995, 1999). The use of vertically averaged vorticity improves temporal coherence in instances where vorticity maxima shift between levels (Hodges et al., 2017).

Cyclone-centred sampling of meteorological fields along cyclone tracks was performed to detect warm-core structures and measure cyclone intensities, following Hodges et al. (2017). For warm-core identification, the T63-truncated vorticity data on seven levels covering 850–250 hPa were added to tracks by recursively searching for a vorticity maximum at each level using the previous level’s maximum as the starting point for a steepest-ascent maximization applied to the B-spline-interpolated field. A search radius of 5° was used, centred on each level’s maximum. For the Southern Hemisphere, fields were scaled by -1 . To quantify cyclone intensity, mean sea-level pressure minima within a radius of 5° and 925-hPa and 10-metre wind speed maxima within a radius of 6° of the storm centre were sampled from reanalysis or model-output fields at their native, non-truncated resolutions. (All radii are geodesic.)

Following Hodges et al. (2017), objective identification of tropical cyclones adhered to the following criteria:

- cyclogenesis equatorward of 30°N
- total cyclone lifetime must exceed two days
- T63 relative vorticity at 850 hPa must exceed $6 \times 10^{-5} \text{ s}^{-1}$

- T63 relative vorticity centre must exist at each level between 850 and 250 hPa to indicate a coherent vertical structure
- T63 relative vorticity decrease with increasing height between 850 and 250 hPa by at least $6 \times 10^{-5} \text{ s}^{-1}$ to indicate the presence of a warm core

The three T63 relative vorticity criteria must also be jointly attained for at least four consecutive time steps (i.e., one day) over ocean only. Together, these criteria minimise inclusion of spurious short-lived or relatively weak vorticity features. The same criteria were used for each reanalysis and model simulation and across all ocean basins.

Crucial to our analyses, vorticity-based tracking and post-tracking identification of tropical cyclones yields longer cyclone lifecycles (compared with central-pressure-based algorithms and methodologies where identification is performed during tracking), which allows for objective analysis of post-tropical storm evolution (Hodges et al., 2017). A comparison of TRACK results with results from a different tracking algorithm, which does not capture the full lifecycle, demonstrates this advantage of vorticity-based tracking (section S1.1; Fig. S1). In addition, filtering gridded data to a common spectral truncation, rather than tuning the cyclone-tracking algorithm to a given dataset, allows both inter-model and inter-resolution comparisons that are not complicated by methodological differences (Hodges et al., 2017). Applying TRACK to a reanalysis globally, as described here, identifies ~30,000 tropical vortices per year. Of these, ~8,000 per year have a lifetime that exceeds two days and are retained; of these, ~120 per year exhibit the warm-core structure of a tropical cyclone (Vannière et al., 2020). Our study is based on recently published tropical cyclone track datasets, derived using a consistent methodology (Roberts et al., 2020a; Roberts et al., 2020b). Sample sizes for all tropical cyclones undergoing ET are given in Table 3. Finally, spatial track statistics—track and genesis densities—were computed using spherical kernel estimators, following Hodges (1996).

| Model name | Atmosphere-only | | Fully coupled | |
|------------------|---------------------------|--------------------------|------------------|-----------------------|
| | <i>highresSST-present</i> | <i>highresSST-future</i> | <i>hist-1950</i> | <i>highres-future</i> |
| CNRM-CM6.1 | 42.3, 52.0 | 41.0, 47.5 | 43.4, 45.8 | 40.1, 39.4 |
| CNRM-CM6.1-HR | 47.9, 55.9 | 46.7, 51.5 | 50.0, 49.6 | 46.8, 42.3 |
| EC-Earth3P | 19.2, 29.3 | 20.1, 28.9 | 19.9, 27.6 | 19.1, 24.0 |
| EC-Earth3P-HR | 30.1, 32.1 | 29.1, 29.4 | 26.6, 28.8 | 26.8, 27.8 |
| ECMWF-IFS-LR | 34.7, 41.6 | n/a | 29.6, 41.5 | n/a |
| ECMWF-IFS-HR | 39.8, 44.6 | n/a | 34.5, 41.7 | n/a |
| HadGEM3-GC3.1-LL | n/a | n/a | 28.4, 38.7 | 28.6, 36.3 |
| HadGEM3-GC3.1-LM | 36.3, 50.0 | 36.5, 50.7 | n/a | n/a |
| HadGEM3-GC3.1-MM | 60.1, 68.8 | 60.9, 65.0 | 55.0, 56.0 | 53.2, 53.4 |
| HadGEM3-GC3.1-HM | 63.8, 69.0 | 63.1, 64.6 | 58.1, 56.4 | 58.9, 54.3 |
| HadGEM3-GC3.1-HH | n/a | n/a | 63.4, 56.2 | 60.1, 52.9 |
| MPI-ESM1.2-HR | 10.5, 16.0 | 9.4, 14.5 | 11.4, 16.9 | 10.4, 15.5 |
| MPI-ESM1.2-XR | 10.1, 17.0 | 9.6, 15.0 | 11.1, 17.4 | 10.1, 14.9 |

Table 3. Annual-mean global sample sizes (cyclones year⁻¹) for all tropical cyclones undergoing ET in each model simulation, given as n_{NH} , n_{SH} .

2.4 Cyclone phase-space analysis

The temporal evolution of cyclone structure, including identifying ET, is quantifiable by analysis of a cyclone's thermal wind fields (Hart, 2003; Hart and Evans, 2001). So-called cyclone phase-space analysis involves three parameters: the thermal axisymmetry of the cyclone (B ; Eq. 1) and the lower- (T_L ; Eq. 2) and upper-tropospheric (T_U ; Eq. 3) cyclone-relative thermal winds. In this study, these parameters were computed using 6-hourly data for all reanalyses and climate models. B is defined as:

$$B = h \left(\overline{Z_{600} - Z_{925}}|_R - \overline{Z_{600} - Z_{925}}|_L \right) \quad (1)$$

where $h = 1$ for the Northern Hemisphere and -1 for the Southern Hemisphere, Z_p is geopotential height (m) at level p (isobaric; hPa), and R and L denote the right- and left-hand semicircles, respectively, relative to the cyclone's displacement direction. In this study, we followed the majority of previous research (Bieli et al., 2019; Bieli et al., 2020; Dekker et al., 2018; Hart, 2003; Liu et al., 2017; Studholme et al., 2015) and defined thermal axisymmetry (i.e., non-frontal) as $B < 10$ and asymmetry (i.e., frontal) as $B \geq 10$ m. To compute T_L and T_U between isobaric surfaces, Hart (2003) used the slope of the linear regression between ΔZ and $\ln p$ as the derivative of ΔZ relative to $\ln p$ to determine the mean ΔZ over a given pressure range. However, to ensure consistency between phase-space parameters computed from reanalyses and model output, and to account for the different pressure levels on which reanalysis and model data are available, it was necessary to adopt a three-level procedure, following recent studies (Bieli et al., 2019; Bieli et al., 2020; Liu et al., 2017; Studholme et al., 2015). Here, T_L (925–600 hPa) and T_U (600–250 hPa) are defined as vertical derivatives of the horizontal geopotential height gradient:

$$T_L \equiv -|V_T^L| = \frac{\partial(\Delta Z)}{\partial \ln p} \Big|_{925 \text{ hPa}}^{600 \text{ hPa}} \quad (2)$$

$$T_U \equiv -|V_T^U| = \frac{\partial(\Delta Z)}{\partial \ln p} \Big|_{600 \text{ hPa}}^{250 \text{ hPa}} \quad (3)$$

where p is pressure and $\Delta Z = Z_{max} - Z_{min}$, where Z_{max} and Z_{min} are the maximum and minimum geopotential height, respectively, at a given level within a 5° radius of the cyclone centre.

Positive T_L or T_U indicates the presence of a warm core in the upper or lower troposphere, respectively; negative values indicate a cold core. A deep warm- or cold-core structure is identified where T_L and T_U have the same sign. We performed phase-space analysis for all reanalyses (section 2.1) and all PRIMAVERA models (section 2.2). In our analysis, cyclone centres in reanalyses and model output are those identified objectively by TRACK, which

ensures dynamical consistency between cyclone positions and the geopotential height field. This differs from Bieli et al. (2020), who centred reanalysis geopotential data on best-track storm locations. The approach taken in our study avoids any potential inconsistencies between reanalysis and best-track storm centres, which would need to be accounted for, particularly at weaker intensities (Hodges et al., 2017).

Among existing studies, various phase-space thresholds have been employed to identify ET (e.g., Bieli et al., 2019; Hart and Evans, 2001; Kofron et al., 2010; Liu et al., 2017; Zarzycki et al., 2017). We defined ET onset as either cold-core development (i.e., $T_L < 0$) or development of thermal asymmetry (i.e., $B \geq 10$), thereby allowing for either ET pathway. ET completion is defined as the first occurrence of both $B \geq 10$ m and $T_L < 0$. These thresholds are suitable for high-resolution gridded data (Michaelis and Lackmann, 2019) and are supported by cluster analysis of observed ET events (Arnott et al., 2004). However, much of the ET-identification literature has focussed on the North Atlantic, yet ET phase-space pathways may differ between ocean basins (Bieli et al., 2019). To account for these difficulties in our global study, ET was identified only where the completion criterion is satisfied for at least four consecutive timesteps (i.e., one day). The use of this additional one-day criterion identifies meaningful temporal changes in B and T_L and avoids counting any spurious, high-frequency temporal variability in phase-space parameters as multiple core-structure changes, following (Baker et al., 2021). An analysis of the sensitivity of ET location to methodological choices is presented in section S1.2, showing a large spread in ET location (Fig. S2). In this study, ET-completion latitude was identified after a warm-core structure persisted for at least 2 days based on phase-space parameters (i.e., $T_L > 0$ and $T_U > 0$), corresponding to ‘w’ in Fig. S2. As such, sample sizes (Table 1 and Table 3) remain unchanged. This method avoids false positives in ET identification arising from tropical depressions and other weak, precursor systems (Bieli et al., 2020), and is therefore more appropriate to analysis of ET location (see section S1.2 for details).

2.5. Identifying post-ET reintensification

Instances of post-ET reintensification were defined as a post-ET increase in p_{min} of at least -4 hPa, a threshold that is based on published case studies (e.g., Zhu et al., 2018), but the number of identified reintensification events is necessarily sensitive to this threshold. For consistency, we applied a single threshold across all reanalyses and models; a higher

threshold will likely be appropriate for any future analysis of higher-resolution (i.e., convection-permitting) models. We used p_{min} to avoid any complications arising from inter-model differences in how near-surface wind speeds are computed (e.g., related to surface roughness).

2.6 Eady growth rate

Eady growth rate maxima (Eq. 4) were computed as (Hoskins and Valdes, 1990):

$$\sigma_{max} = 0.31 \frac{f}{N} \frac{\partial(u,v)}{\partial Z} \quad (4)$$

where f is the Coriolis parameter, N is the static stability parameter, Z is geopotential height, and u and v are the zonal and meridional winds, respectively, which were used to compute the magnitude of the horizontal wind (i.e., $\sqrt{u^2 + v^2}$). The vertical derivatives, $\partial(u,v)$ and ∂Z , were computed between the 850- and 250-hPa levels using 6-hourly data.

3. Results

In each of the following sections, we present historical results and model evaluation followed by analysis of projected future changes out to 2050.

3.1 Spatial cyclone statistics

We first present spatial track density patterns for tropical cyclones undergoing ET in reanalyses and simulated across the PRIMAVERA ensemble. Reanalyses exhibit a high degree of consistency for track density and demonstrate that tropical cyclones undergo ET in all ocean basins. However, fewer ET events are identified over the Northern Indian Ocean (Fig. 1a), where relatively low-latitude landfall either disrupts liminal ET events or averts potential ET cases altogether, primarily via boundary-layer frictional effects (Bieli et al., 2019). Overall, basins' climatological ET activity is proportional to their tropical cyclone activity. The highest ET frequencies are identified in both the Western North Pacific and South Pacific basins, with climatological mean values of ~ 12 cyclones year⁻¹. The North Atlantic is the most active basin for ET outside the Pacific, and comparably low activity occurs across the South Atlantic and South Indian basins (Fig. 1a).

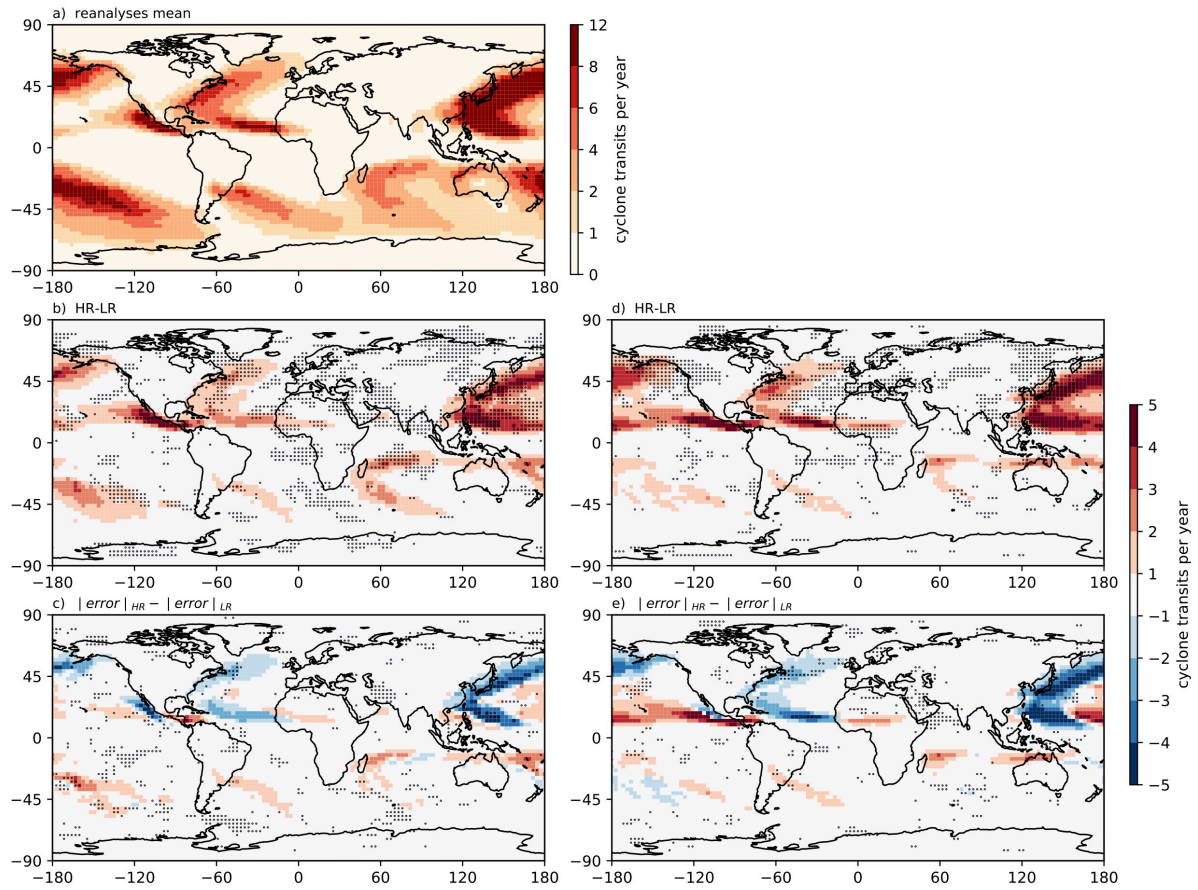


Fig. 1. Cyclone track density for all tropical cyclones undergoing ET. (a) Multireanalysis mean, (b–c) *highresSST-present* and (d–e) *hist-1950*. Track density was computed from complete tracks, including precursor stages, and is shown in units of cyclone transits per year per unit area (within a 5 ° geodesic radius of storm centres). All available reanalysis years (Table 1) are included in this analysis. (b, d) HR–LR denotes the ensemble-mean difference between high and low resolution. (c, e) $|error|_{HR} - |error|_{LR}$ denotes the ensemble-mean difference of the absolute error (model versus multireanalysis mean) between high and low resolution. The low-resolution (‘LR’) sub-ensemble includes CNRM-CM6.1-LR, EC-Earth3P-LR, ECMWF-IFS-LR, HadGEM3-GC3.1-LM(-LL), and MPI-ESM1.2-HR. The high-resolution (‘HR’) sub-ensemble includes CNRM-CM6.1-HR, EC-Earth3P-HR, ECMWF-IFS-HR, HadGEM3-GC3.1-HM(-HH), and MPI-ESM1.2-XR. In b)–e), stippling indicates where all five models agree on the sign of the difference.

The frequency of ET events simulated by PRIMAVERA models increases when resolution is increased from ~ 100 km to ~ 25 km in all basins, both in the *highresSST-present* (Fig. 1b) and *hist-1950* (Fig. 1d) experiments. Ensemble-mean climatologies are similar between both experiments (Fig. S3). The North Atlantic and Western North Pacific basins are regions of relatively widespread inter-model agreement on the sign of this resolution-sensitivity in track density, again regardless of whether SST is prescribed. When prescribed, inter-model agreement is also identified in the South Pacific and South Indian basins (Fig. 1b). This result is consistent with a recent equivalent analysis of all tropical cyclones in PRIMAVERA simulations (Roberts et al., 2020a), where increased frequencies were simulated at higher model resolution across all ocean basins, for which the leading explanation is that finer atmospheric resolution increases the conversion rate of precursor vortices (or ‘seeds’) to tropical cyclones (Roberts et al., 2020a; Vecchi et al., 2019; Vidale et al., 2021). Tropical-cyclone intensities simulated at model resolutions in the range 50–20 km are more comparable with observational estimates (Roberts et al., 2020a), due in part to enhanced surface latent heat flux (Vannière et al., 2020), implying that a more realistic proportion may withstand midlatitude environmental conditions hostile to tropical cyclones prior to and during the initial stages of ET. At low resolutions (typically ~ 100 km), PRIMAVERA models simulate too few ET systems compared with reanalyses, particularly across the North Atlantic and Western North Pacific, in both the *highresSST-present* (Fig. S4a) and *hist-1950* (Fig. S4c) experiments. Increasing resolution to ~ 25 km leads to increased track density globally, reducing negative biases in these basins but engendering positive biases in the Eastern North Pacific and South Pacific (Fig. S4c, d). In *hist-1950*, this bias reduction is consistent with a reduction in negative surface temperature biases at high resolution (e.g., ~ 1 °K reduction in the North Atlantic; Moreno-Chamarro et al., 2022). In section 3.2, we examine ET frequency and the percentage of tropical cyclones undergoing ET separately.

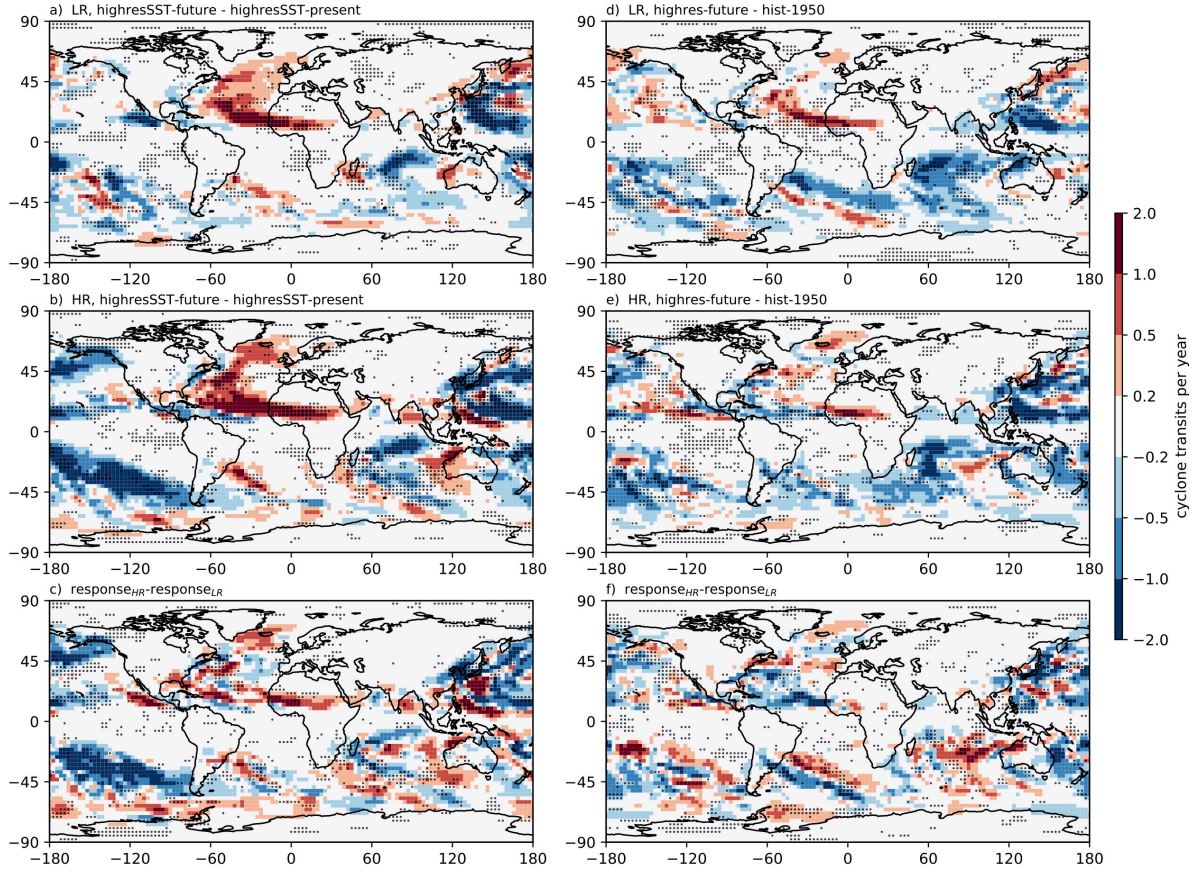


Fig. 2. Climate-change response of track density for all cyclones undergoing ET. (a–c) *highresSST-future* minus *highresSST-present* and (d–f) *highres-future* minus *hist-1950*. Track density was computed from complete tracks, including precursor stages, and is shown in units of cyclone transits per year per unit area (within a 5 ° geodesic radius of storm centres). The low-resolution (‘LR’) sub-ensemble includes CNRM-CM6.1-LR, EC-Earth3P-LR, HadGEM3-GC3.1-LM(-LL), and MPI-ESM1.2-HR. The high-resolution (‘HR’) sub-ensemble includes CNRM-CM6.1-HR, EC-Earth3P-HR, HadGEM3-GC3.1-HM(-HH), and MPI-ESM1.2-XR. Stippling indicates where all models agree on the sign of the difference.

Overall, PRIMAVERA simulations indicate that increasing resolution improves the representation of ET frequency, as measured by track density, particularly across the North Atlantic and Western North Pacific (Fig. 1c, e). For these basins, reductions in ensemble-mean absolute biases are found in both *highresSST-present* and *hist-1950*, and areas of bias reduction across multiple models occur primarily over western boundary currents—the Gulf Stream and Kuroshio, respectively. That these regions of resolution-dependence and reduced biases overlap indicates that capturing the sharpness of SST fronts and associated baroclinicity is important in simulating ET (Evans et al., 2017; Klein et al., 2002), and, consistent with this, we find enhanced meridional SST gradients in both of these boundary-current regions (Fig. S5). In the Southern Hemisphere, little difference in ensemble-mean biases is found between resolutions, with a caveat that observational or reanalysis-based climatologies for the Southern Ocean are themselves more uncertain (Hodges et al., 2017). The PRIMAVERA ensemble provides evidence that atmospheric resolutions typical of CMIP6 are too coarse to adequately capture basin-mean tropical-cyclone (Roberts et al., 2020a) and ET statistics (this study). Increasing resolution to ~25 km partly addresses this shortcoming.

The climate-change response of track density for tropical cyclones undergoing ET in high-resolution simulations is basin-dependent, with differences between atmosphere-only and fully coupled simulations also apparent. In *highresSST-future*, increased track density is simulated across the North and South Atlantic (but decreased over the eastern United States) and over the Maritime Continent; decreases are simulated over the Eastern and Western North Pacific and South Indian basins; and an unclear, mixed response characterises the North Indian Ocean (Fig. 2a–b). Inter-model agreement about the sign of these changes is largely confined to cyclogenesis regions (e.g., equatorial West Africa) and over the Gulf Stream and Kuroshio Current. In *highres-future* simulations, positive climate-change responses are confined to the central and Eastern North Pacific. The spatial response pattern over the North Atlantic—increased over central and eastern North Atlantic and decreased along the United States’ east coast—is similar between *highresSST-future* and *highres-future*, but the magnitude of the response is reduced in the fully coupled simulations (Fig. 2d–f). This spatial pattern is supported by recent projections, with increases particularly apparent in the eastern North Atlantic (Liu et al., 2017), consistent with the projected eastward and poleward expansion of cyclogenesis within this basin (Haarsma et al., 2013).

Increasing horizontal resolution has a localised effect on the climate-change response of track density for ET (Fig. 2c, f). In *highresSST-future*, resolution-sensitive responses to climate change, which are common across *all* models, are seen only over the central North Atlantic and parts of the Southern Ocean. In *highres-future*, spatially coherent and resolution-sensitive responses to climate change are seen over the South Atlantic and Eastern North Pacific basins, where simulated track density maxima are shifted equatorward at high resolution. However, the spatial patterns of resolution sensitivity over the North Atlantic and Western North Pacific broadly resemble the spatial climate-change response patterns, which indicates that these responses are enhanced at high resolution in most models. This is seen more clearly in the atmosphere-only experiment (Fig. 2c) than in the fully coupled experiment (Fig. 2f).

3.2 Interannual variability in ET

Over the period 1979–2018, high-resolution *highresSST-present* simulations reproduce the multireanalysis-mean climatological ET counts for Northern Hemisphere basins (Fig. 3, left), except for the Northern Indian Ocean, a basin where few ET events occur. However, little improvement with increased resolution is seen for Southern Hemisphere basins (Fig. 3, left). Again, uncertainty is higher across the Southern Ocean, with greater inter-reanalysis spread seen for Southern Hemisphere basins. These results are also true of the *hist-1950* simulations (Fig. 4, left). The *highresSST-present* simulations appear to capture decadal variability in the role of SST in sustaining tropical cyclones to ET. In certain basins, periods are apparent where the *highresSST-present* ensemble mean and multireanalysis mean ET count match well: e.g., 1985–2000 for the North Atlantic and 1990–2005 for the Western North Pacific (Fig. 3, left). These periods coincide with observed positive phases in Atlantic Multidecadal Variability and Pacific Decadal Oscillation, respectively. For ET %, differences between low- and high-resolution ensemble means are small for most basins (Fig. 3, right). This suggests that the large-scale environmental conditions conducive to ET are not substantially different across the range of model resolutions considered here. This indicates that increased ET frequency at high resolution is driven primarily by increased tropical cyclone frequency, not by an increase in ET %. Similar mean values and variance in ensemble-mean ET count and ET % are simulated in both *highresSST-present* (Fig. 3) and *hist-1950* (Fig. 4) experiments.

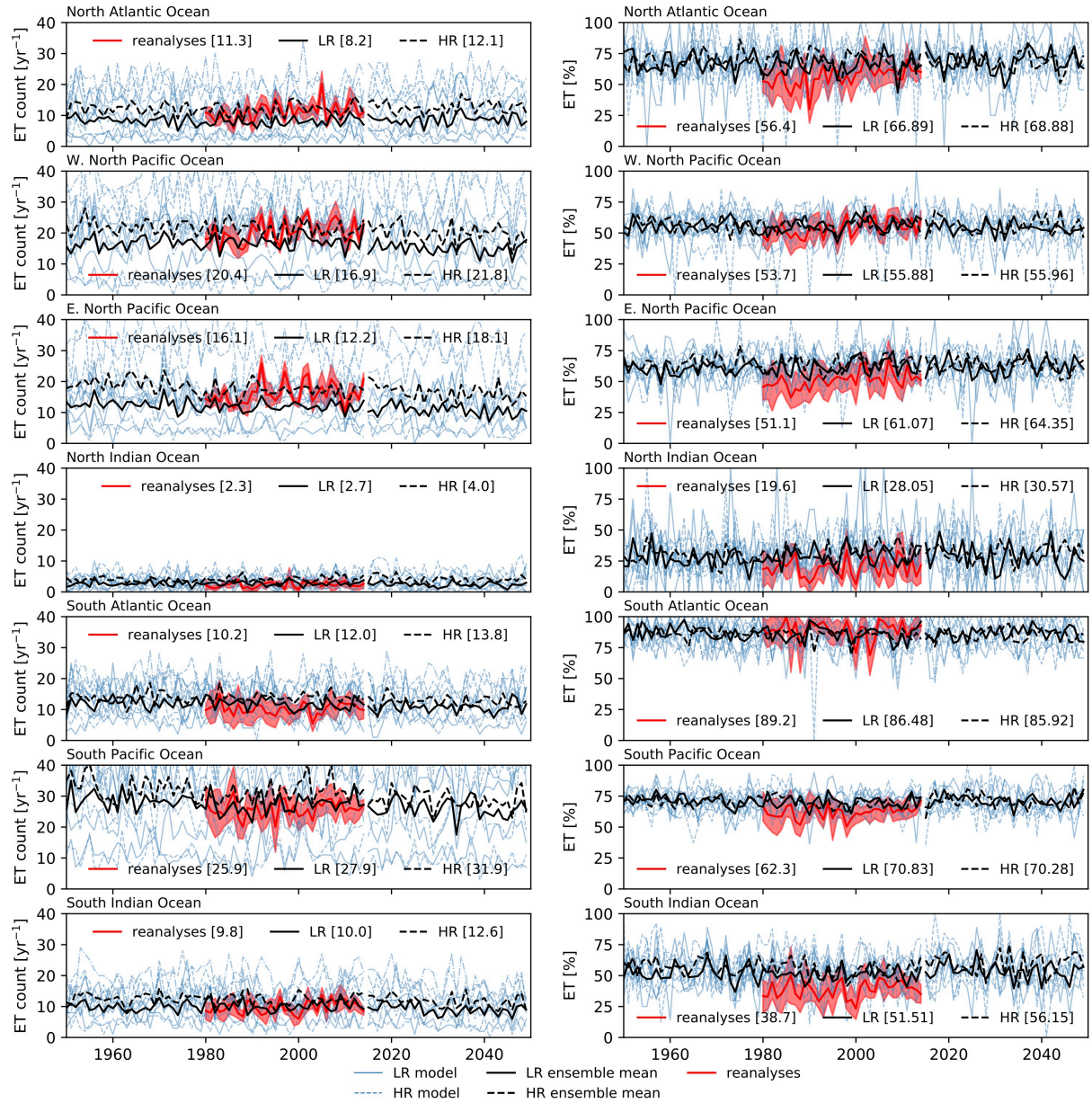


Fig. 3. Interannual variability in (left) the number of ET events and (right) the percentage of tropical cyclones undergoing ET in each ocean basin in reanalyses and simulated in *highresSST-present* and *highresSST-future* experiments. Shown are (red) the multireanalysis mean, with 1 standard deviation of the reanalysis spread indicated by red shading, and (solid black) low- and (dashed black) high-resolution ensemble means. Each panel's legend gives climatological-mean values of (left) ET count or (right) ET % for the reanalyses and historical simulations. Also shown are (blue) timeseries for individual simulations to indicate the ensemble spread for each basin.

In *highresSST-present*, models' skill in reproducing the multireanalysis-mean interannual variability in ET count varies between basins (Table 4). Interannual variability in ensemble-mean and multireanalysis-mean ET counts are significantly, positively correlated for three basins at low resolution and four basins at high resolution. The North Atlantic and Western North Pacific basins are significantly correlated at both resolutions; the South Atlantic and South Pacific basins are significantly correlated only at high resolution; and the Eastern North Pacific is significant only at low resolution. Only for the North and South Indian basins is ensemble-mean variability uncorrelated with reanalyses at either resolution. (Correlation coefficients for *hist-1950* simulations are not shown because it is not expected that fully coupled models' internal year-to-year variability would mimic that of forced simulations or reanalyses.) For ET %, fewer significant correlations are found between ensemble-mean and multireanalysis-mean timeseries (Table 4). Positive correlations are seen in the Northern and Southern Indian basins and in the South Pacific basin at high resolution. However, low- and high-resolution ensemble-mean ET % timeseries covary in most basins in both *highresSST-present* (Fig. 3) and *hist-1950* (Fig. 4), more so than for ET count. To explain this, we hypothesise that the large-scale environment conducive to the baroclinic conversion of tropical cyclones is less sensitive to model resolution, while ET count depends on tropical cyclone count, which is sensitive to model resolution (Roberts et al., 2020a).

Recent analysis of an ensemble of HadGEM3-GC3.1 simulations, performed under HighResMIP, demonstrated that mean skill in representing interannual variability in tropical cyclone count improves with additional members (Roberts et al., 2020a). At present, the required six-hourly geopotential outputs are available for too few ensemble members to repeat such an analysis for tropical cyclones undergoing ET, but this would constitute valuable future work when sufficient model output is obtainable. Nonetheless, quantifying the level of skill that exists in capturing interannual variability in the subset of tropical cyclones that undergo ET, while lower than that for all tropical cyclones, is important, establishing the baseline for HighResMIP-class models. This prompts further examination of ET seasonality in the historical and future atmosphere-only simulations, which is possible in the continuous PRIMAVERA simulations.

| Ocean basin | ET count | | ET % | |
|-----------------------|-------------|-------------|-------------|-------------|
| | LR | HR | LR | HR |
| North Atlantic | 0.31 | 0.30 | 0.24 | -0.16 |
| Western North Pacific | 0.50 | 0.34 | 0.21 | 0.24 |
| Eastern North Pacific | 0.43 | 0.22 | 0.42 | 0.16 |
| North Indian | -0.08 | 0.03 | 0.03 | 0.38 |
| South Atlantic | 0.07 | 0.34 | 0.12 | 0.27 |
| South Pacific | 0.08 | 0.50 | 0.17 | 0.34 |
| South Indian | -0.04 | -0.19 | 0.24 | 0.33 |

Table 4. Pearson’s r coefficients for correlations between low- (LR) or high-resolution (HR) ensemble-mean and multireanalysis-mean interannual variability in ET count and ET % for each ocean basin. Coefficients are shown only for *highresSST-present*; *hist-1950* simulations are not shown because it is not expected that coupled models’ internal year-to-year variability would mimic that of forced simulations or reanalyses. Significant ($p < 0.1$) correlations are in bold type.

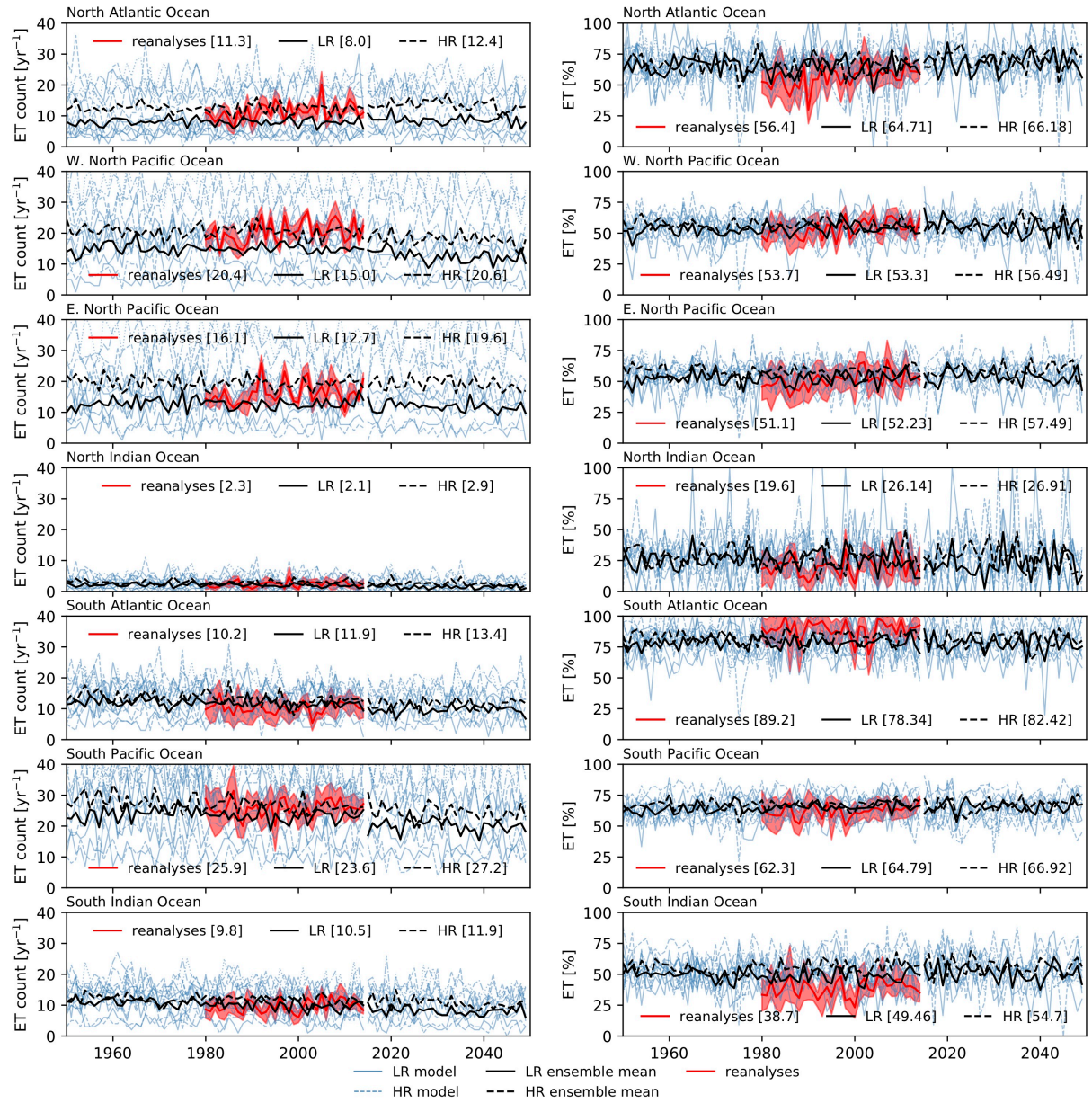


Fig. 4. As in Fig. 3 for fully coupled *hist-1950* and *highres-future* simulations.

3.3 Historical and future ET seasonality

We next evaluate the seasonal cycle of ET, focussing on the North Atlantic and Western North Pacific basins for which both climatological ET statistics (Fig. 1) and interannual ET variability (Table 4) are represented reasonably across models. In the North Atlantic, reanalyses show ET % increasing from July to a peak in September before declining into winter (Fig. S6a). In the *highresSST-present* experiment, most models reproduce this seasonality, but the magnitude of the seasonal peak is overestimated by ~10 % at high-resolution. There are indications that increased atmospheric resolution improves the simulation of the timing of the seasonal ET % peak. Two models—CNRM-CM6.1 and EC-Earth3P—simulate the seasonal peak too early (in August) at low resolution but simulate a later peak (in September) at high resolution. Additionally, MPI-ESM1.2, the lowest-resolution model in this ensemble, simulates comparably muted seasonality that also peaks earlier than reanalyses at both resolutions. In the fully coupled *hist-1950* experiment, models reproduce the multireanalysis-mean seasonal cycle, but HadGEM3-GC3.1 and CNRM-CM6.1 simulate a broader seasonal distribution compared with reanalyses (Fig. S7a). In the Western North Pacific, reanalyses show bimodal seasonality, with peaks in ET % in May and September (Fig. S6b). Excepting the MPI-ESM1.2 model, which does not capture bimodality, *highresSST-present* simulations also exhibit two seasonal peaks, but each occurs one to two months later than in reanalyses in both low- and high-resolution integrations (Fig. S6b), and this also holds true for *hist-1950* simulations (Fig. S7b).

To assess any potential future change in seasonality, ΔET %, we differenced the historical and future seasonal cycles. For the North Atlantic, despite pronounced inter-model spread throughout most of the annual cycle, there is an indication of more consistent model behaviour during August–November, months for which most models simulate an increase in ET % in both the *highresSST-future* (Fig. S6c) and *highres-future* experiments (Fig. S7c). To quantify the degree to which this inter-model consistency represents secular change in ET seasonality, the annual fraction of total annual ET events occurring during August–November was computed. A significant, positive trend in this quantity over the period 1950–2050 is found in the ensemble mean of high-resolution atmosphere-only simulations (Fig. 5a), but the trend is not significant in reanalyses, which likely cover too short a period (1980–) to assess secular change, and is significant in the low-resolution ensemble mean only at the 80 % level. In fully coupled simulations, no significant trends are seen (Fig. S8a). Conducting a similar analysis of the forthcoming extension of ERA5 back to 1950 is warranted, pre-satellite observational uncertainty notwithstanding. For the Western North Pacific, the inter-model spread during the annual cycle of ΔET % is similar between *highresSST-future* (Fig. S6d) and *highres-future* simulations (Fig. S7d) and, in contrast to the North Atlantic, no significant secular change in ET seasonality is found in either reanalyses or in PRIMAVERA simulations out to 2050 (Fig. 5b and Fig. S8b). However, together with projected changes in track density (Fig. 2a–b, d–e), these results provide further evidence that the future response of ET to climate change across the North Atlantic differs from that of the Western North Pacific and of other ocean basins. Therefore, we next investigate the role of cyclone structure in explaining these distinct North Atlantic and Western North Pacific responses.

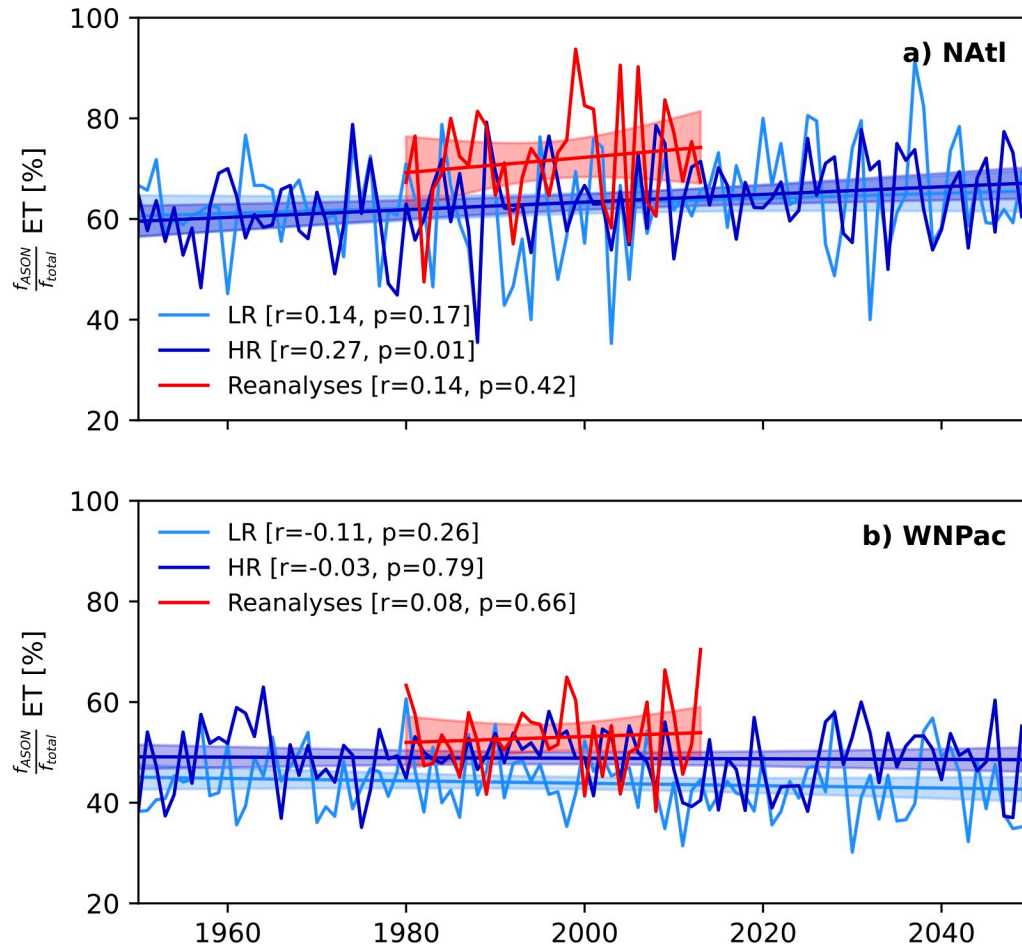


Fig. 5. Secular change in the proportion of ET events occurring during August–November in reanalyses (red) and low- (pale blue) and high-resolution (dark blue) atmosphere-only simulations (ensemble mean) for the (a) North Atlantic and (b) Western North Pacific basins. Shading shows the 95 % confidence interval for the linear fit. ECMWF-IFS is not included in this analysis because no future simulations were performed in HighResMIP for this model.

3.4 Response of cyclone structures to climate change

To examine the response of cyclone core structure to climate change, we computed ensemble-mean bivariate frequency distributions of phase-space parameters, B , T_L , and T_U in the high-resolution simulations. The T_L – B distribution exhibits a similar general structure in the *highresSST-present* and *-future* experiments for both the North Atlantic (Fig. 6a–b) and Western North Pacific (Fig. 6d–e) basins. This is also true for T_L – T_U distributions (Fig. 7a–b and Fig. 7d–e). Generally, tropical cyclones undergoing ET occupy the lower-right (symmetric, warm core) and upper-left (asymmetric, cold core) quadrants, with fewer instances in either hybrid (transitional) quadrant. The phase-space parameter distributions simulated across PRIMAVERA models are consistent with previous studies (Hart et al., 2006; Michaelis and Lackmann, 2019). Historical ensemble-mean values of B and T_L for the North Atlantic are consistent with recent analysis of observations (Studholme et al., 2015) as well as reanalyses and Community Atmosphere Model simulations at resolutions of 55 and 28 km (Zarzycki et al., 2017). Ensemble-mean T_U values are also consistent with these existing studies, except that deep warm-core structures are less frequent in PRIMAVERA models than in recent 15-km-resolution simulations with the Model for Prediction Across Scales–Atmosphere model (Michaelis and Lackmann, 2019), likely due to differences in atmospheric resolution. For the Western North Pacific, model-simulated phase-space parameters are consistent with reanalysis-based values (Kitabatake, 2011). In the fully coupled simulations, T_L – B distributions for both basins are similar to those of the atmosphere-only simulations (Fig. 8c, f), but differences in ensemble-mean T_U values are seen, with warm-core responses to climate change occurring variously throughout the troposphere (Fig. 9c, f).

Under climate change, models forced by prescribed SST simulate stronger warm-core structures in the North Atlantic, indicated by a shift towards higher T_L for axisymmetric tropical cyclones (Fig. 6c). Moreover, T_L – T_U distributions show that the future shift to stronger warm-core structures is primarily confined to the lower troposphere (Fig. 7c, f). (Here, ‘strong’ refers to ensemble-mean T_L values at the higher end of the historical distributions, in which a range of model-simulated intensities are averaged.) These findings are supported by a recent single-model study (Michaelis and Lackmann, 2019), albeit the ensemble-mean signal we report is less pronounced, and are consistent with increased low-level moisture and the potential for enhanced latent heat release in a warmer climate. Future changes in core structures offer a partly mechanistic explanation of the projected increase in

ET across the North Atlantic (Baatsen et al., 2015; Haarsma et al., 2013; Liu et al., 2017) as well as the projected change in track density, which is largely unique to the North Atlantic (Fig. 2a–b, d–e). The lesser energy of weak warm-core cyclones is more likely to dissipate before ET may occur, but relatively strong warm-core structures make cyclones more resilient to unfavourable midlatitude environmental conditions (primarily cooler SST and increased vertical wind shear), prolonging their poleward propagation and making ET more probable across the North Atlantic (Hart et al., 2006).

In the North Pacific, however, this future shift to stronger warm cores is not seen in PRIMAVERA models (Fig. 6f), although more frequent asymmetric, warm-core hybrid structures (upper-right quadrant) in the future are simulated. These instances of hybrid structures show cyclones existing more frequently in the transitional quadrants, potentially indicating a future elongation of ET time (Zarzycki et al., 2017) and an increase in warm-seclusion occurrences, which involve multiple transitions (Baker et al., 2021; Dekker et al., 2018). Also seen is a shift towards stronger upper-level, cold-core structures (Fig. 7f). The Western North Pacific is therefore characterised by more mixed future changes in core-structure frequencies, consistent with the projected response of track density, which generally decreases across the basin but increases in localised areas (Fig. 2b, e). Broadly, these results are also consistent with the lack of any consensus in published projections of ET frequency across the Western North Pacific: both a less favourable future ET environment (Ito et al., 2016) versus moderate future increase in ET frequency (Bieli et al., 2020) have been suggested. For both basins, future phase-space changes in the fully coupled simulations resemble those seen in the atmosphere-only experiments, but the North Atlantic climate-change signal is comparably muted (Fig. 8c, f; Fig. 9c, f).

Overall, these results help clarify the potential role that the climate-change response of cyclones' core structures have in determining future ET frequency changes, and quantifies how this differs between basins. Differences in pre-ET structures potentially underpin basin-specific responses of ET to climate change, and consistency exists among PRIMAVERA models. However, to fully explain what drives disparate North Atlantic and Western North Pacific responses, further studies of future changes in cyclogenesis and midlatitude large-scale conditions are needed, based on models of higher resolution than those in PRIMAVERA, which better simulate the most intense systems (Judt et al., 2021), and, potentially, their interactions with the large-scale environment.

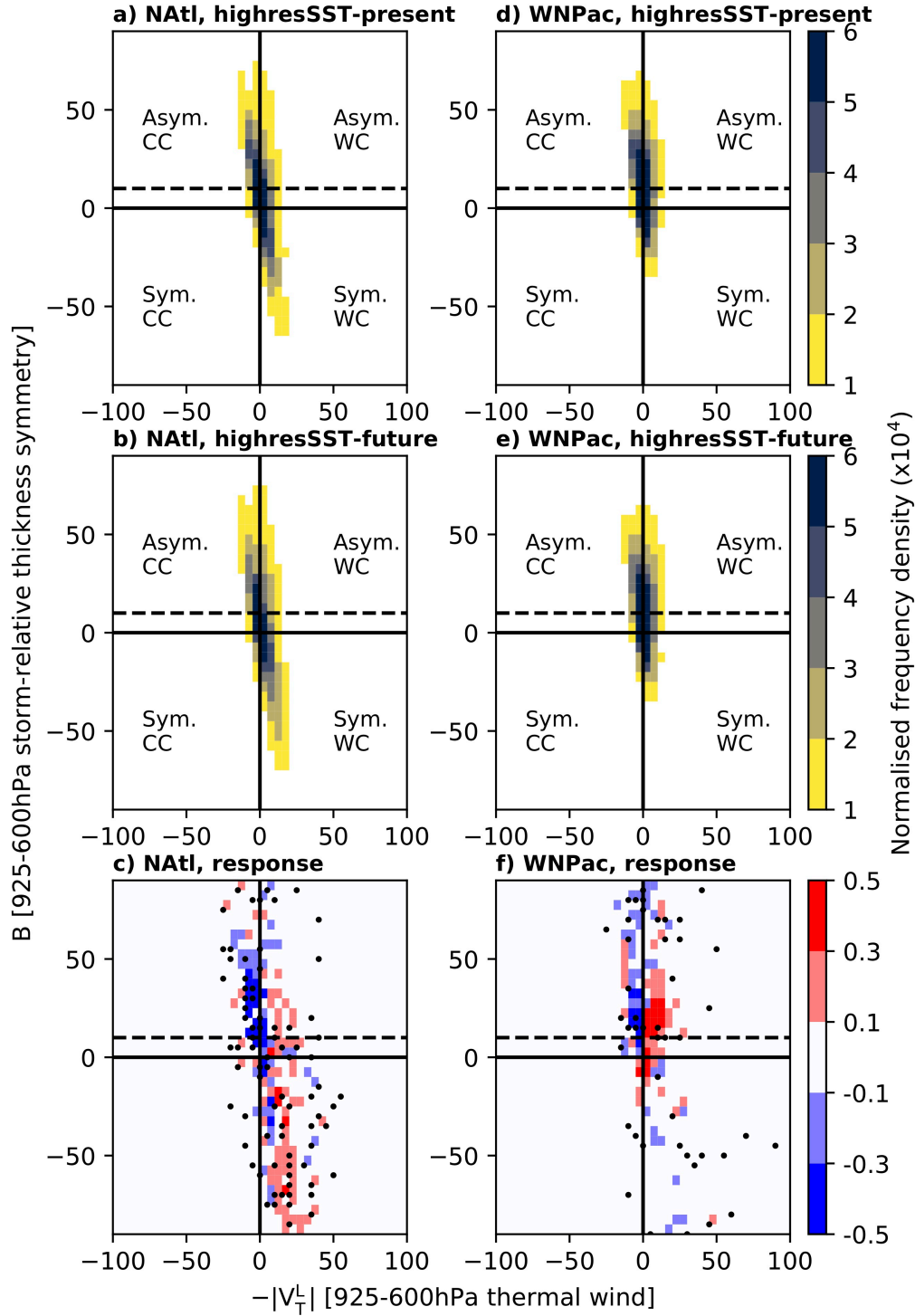


Fig. 6. Ensemble-mean distributions of T_L versus B in high-resolution (a, d) *highresSST-present* and (b, e) *-future* simulations as well as (c, f) the climate-change response for the North Atlantic ('NAtl') and Western North Pacific ('WNPac'). Distributions are computed from every 6-hourly point during the entire lifetime of all storms undergoing ET, plotted as two-dimensional histograms, and normalised by the total number of cyclones (sample sizes for each model are given in Table 3). Values are scaled by 10^4 . Cyclone phase-space

658 categories are warm- ('WC') or cold-core ('CC') and either symmetrical (i.e., non-frontal;
659 'Sym.') or asymmetrical (i.e., frontal; 'Asym.'). The threshold of 10 m used to distinguish
660 thermally symmetric from asymmetric cyclones is indicated (dashed line). Stippling in c) and
661 f) indicates where all models agree on the sign of the difference.
662

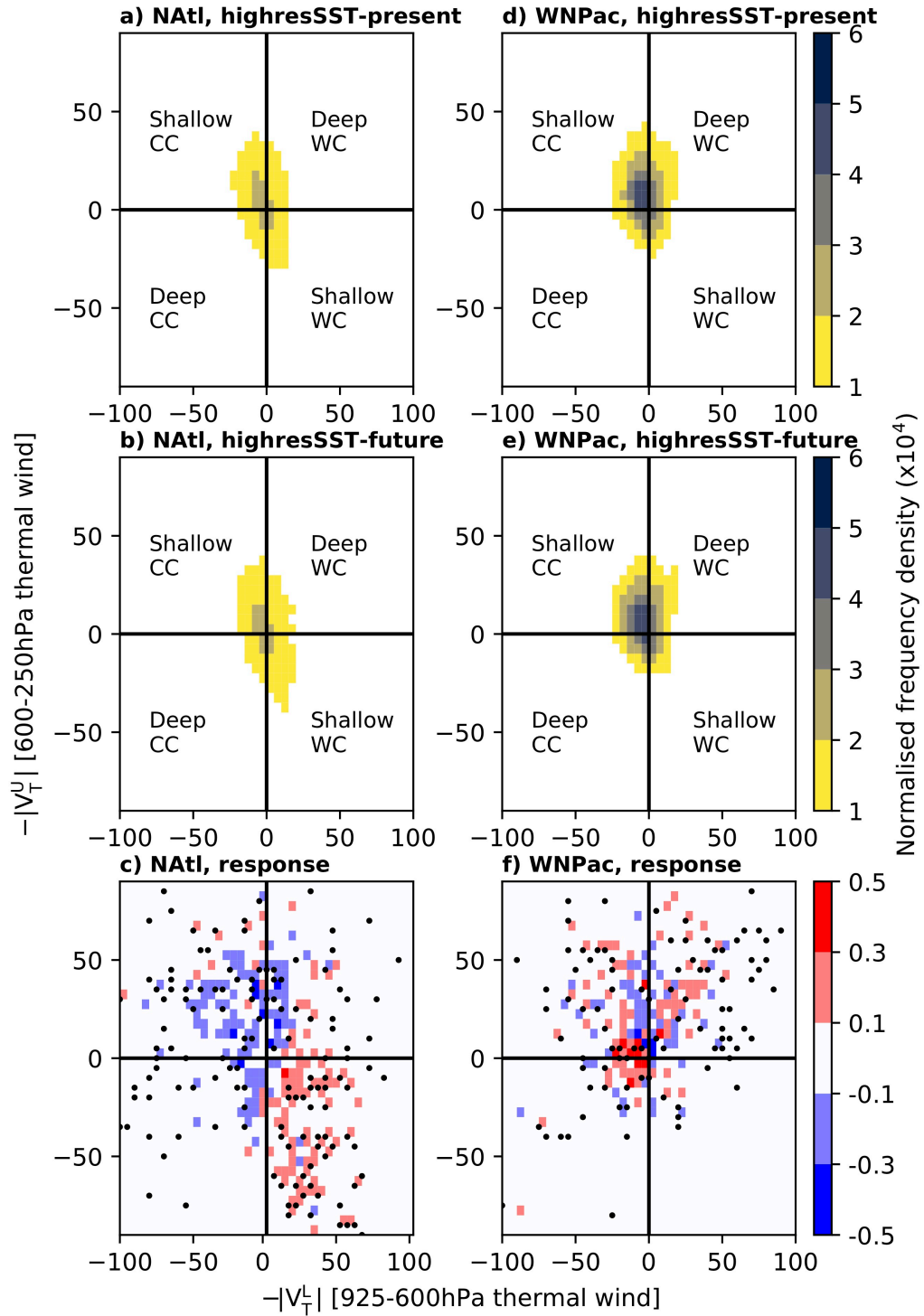


Fig. 7. Ensemble-mean distributions of T_L versus T_U in high-resolution (a, d) *highresSST-present* and (b, e) *-future* simulations as well as (c, f) the climate-change response for the North Atlantic ('NAtl') and Western North Pacific ('WNPac'). Distributions are computed from every 6-hourly point during the entire lifetime of all storms undergoing ET, plotted as two-dimensional histograms, and normalised by the total number of cyclones (sample sizes for each model are given in Table 3). Values are scaled by 10^4 . Cyclone phase-space

670 categories are shallow or deep warm- ('WC') or cold-core ('CC'). Stippling in c) and f)
671 indicates where all models agree on the sign of the difference.
672

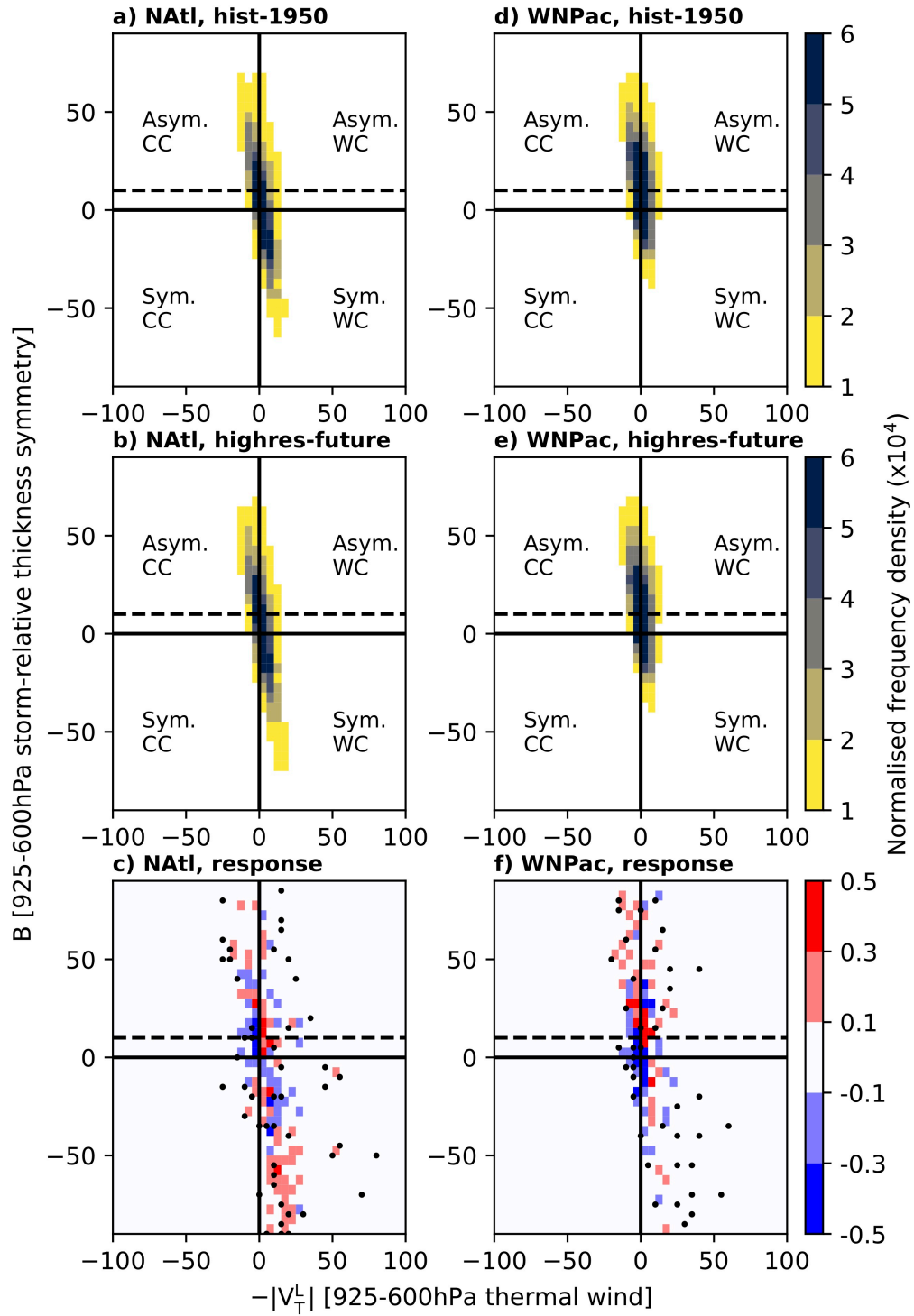


Fig. 8. As in Fig. 6 for *hist-1950* and *highres-future* experiments.

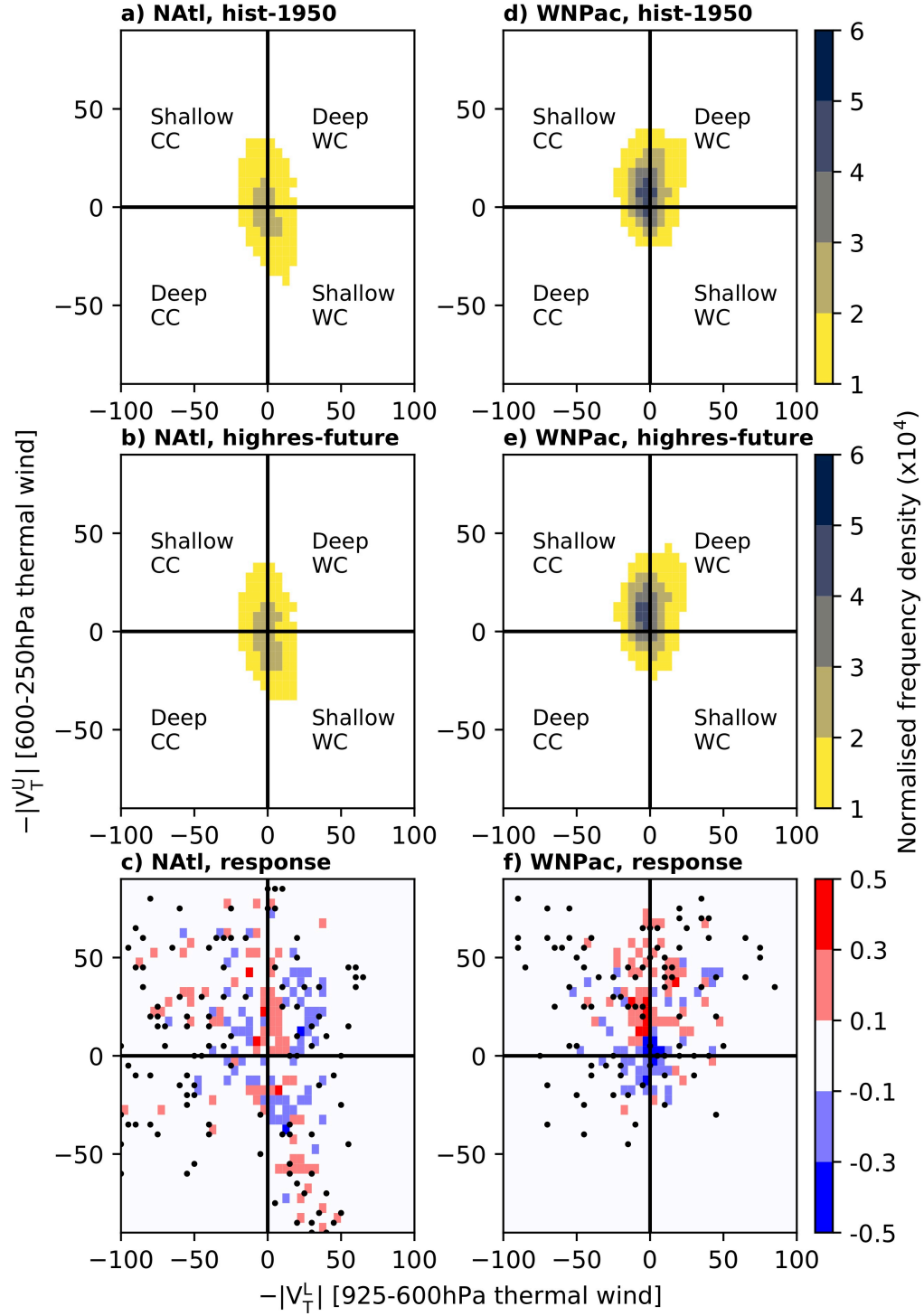


Fig. 9. As in Fig. 7 for *hist-1950* and *highres-future* experiments.

3.5 Pre- and post-ET cyclone intensity

During ET, cyclones develop low-level frontal structures and their horizontal size increases (Evans et al., 2017). As such, increasing model resolution is expected to impact the simulation of cyclones pre- and post-ET differently, particularly in models whose effective resolutions coarsen equatorward. However, performing a global analysis of the pre- and post-ET stages of tropical cyclones' lifecycles is not trivial because ET pathways (i.e., the order in which B and T_L changes occur) differ between ocean basins (Bieli et al., 2019). We therefore separated cyclone tracks' warm- and cold-core stages about ET completion, when both B and T_L satisfy ET criteria, following the definition first used by Hart (2003). Our additional 1-day criterion (see Methods) helps increase confidence in the following inter-model comparison.

Compared with best-track intensity estimates, certain atmosphere-only models (particularly CNRM-CM6.1) simulate realistic intensities at resolutions in the range 20–50 km (Roberts et al., 2020a). However, best-track intensity estimates are not well suited to evaluating post-ET systems (Velden et al., 2006), and the available primary cyclone wind-speed observations, such as satellite scatterometry data, seldom include cyclones' post-tropical stages and span too short a temporal range for climatological evaluation. We therefore turn to reanalyses, which are constrained by observational data, to provide a homogeneous global reference. An important caveat, however, is the underestimation of cyclone wind speeds in reanalyses (Hodges et al., 2017; Murakami, 2014), although this underestimation is less marked at higher latitudes (Sainsbury et al., 2020).

Considering all storms globally, PRIMAVERA models reproduce the reanalyses' cold-core, post-ET intensity distributions at both low and high resolution and in both atmosphere-only and fully coupled simulations (Fig. 10 and Fig. 11, top rows). However, models' representation of warm-core, pre-ET distributions improve markedly with increasing resolution, especially for CNRM-CM6.1 and HadGEM3-GC3.1, but more clearly so in the atmosphere-only than in the fully coupled simulations, wherein cold-wake feedbacks reduce upper-ocean temperatures and weaken subsequent tropical cyclones (Balaguru et al., 2014). Sensitivity to resolution is similar in the fully coupled CNRM-CM6.1 and HadGEM3-GC3.1 simulations (Fig. 11, top row). These results show that horizontal resolutions typical of CMIP6 appear sufficient to simulate cold-core (post-ET) intensity distributions, including the relatively high-intensity tail—resolutions at which large-ensemble studies to quantify multiannual variability of the strongest post-ET storms are computationally feasible.

However, among high-resolution PRIMAVERA models, the high-intensity tail of the warm-core distribution is reproduced only by CNRM-CM6.1.

For *highresSST-future*, several models project decreasing warm-core and increasing cold-core intensities for weaker storms ($<17\text{ms}^{-1}$) but simulate opposite warm- and cold-core responses for stronger storms ($\geq 17\text{ms}^{-1}$) (Fig. 10, bottom row). This warm-core response is consistent with projections of intensified tropical cyclones under anthropogenic warming (Knutson et al., 2020). However, these responses are not replicated by fully coupled models (Fig. 11, bottom row), in which intensity changes are weak (Roberts et al., 2020b). In the fully coupled simulations, the responses of pre- and post-ET intensity distributions to climate change are equivocal, with substantial inter-model differences. We speculate that the climate-change forcing out to 2050 in the HighResMIP experimental protocol is insufficiently strong (i.e., the future simulation period is too short) for a clear signal to emerge. However, it is unclear whether intensity changes would be seen. For tropical cyclones overall, Roberts et al. (2020b) found a weak future intensification in these simulations, and Bieli et al. (2020) found equivocal ET climate-change responses in many basins out to 2100 under the weaker RCP4.5 scenario. If a clear climate-change signal were to emerge with further increases in model resolution, which would increase the relative difference between the weakest and strongest simulated tropical cyclones, this would suggest that processes important for intensity change are not adequately captured at ~ 25 km resolution.

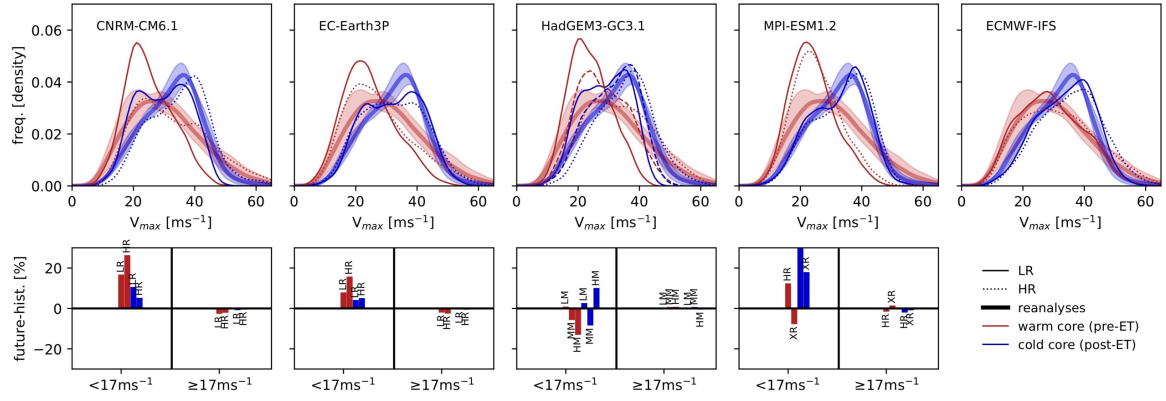


Fig. 10. Intensity (v_{max} at 925hPa) distributions in atmosphere-only simulations for all cyclones undergoing ET globally. For each model, historical simulations are shown in the top row and future simulations in the bottom row. Multireanalysis-mean curves (thick, solid lines) are shown with 1 s.d. (shading). Both low- (thin, solid lines) and high-resolution (thin, dashed lines) simulations are shown. Climate-change responses (i.e., *highresSST-future* minus *highresSST-present*), computed as integrated differences, are shown as percentages for storms whose lifetime-maximum intensity is $<17 \text{ ms}^{-1}$ or $\geq 17 \text{ ms}^{-1}$ for each atmospheric model resolution (ordered left to right).

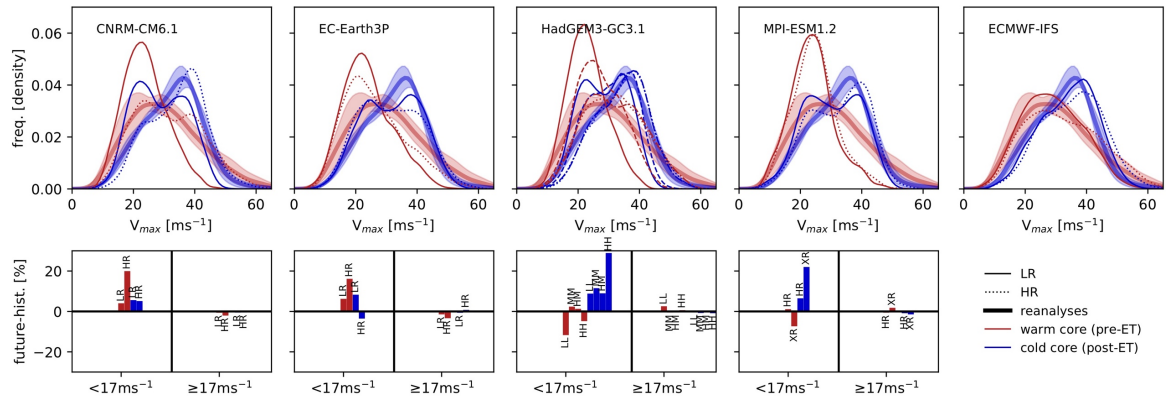


Fig. 11. As in Fig. 10 for fully coupled simulations.

3.6 Post-ET reintensification

The lifetime-maximum intensity of transitioning tropical cyclones typically occurs during the warm-core, tropical phase. However, the addition of a baroclinic energy source and cyclone-wave interactions induce post-ET reintensification (Evans et al., 2017). We quantified the frequencies of reintensifying versus non-reintensifying cyclones in reanalyses and in the PRIMAVERA ensemble. Globally, reanalyses indicate that approximately 50 % of tropical cyclones that undergo ET undergo post-ET reintensification (Fig. 12a). For the North Atlantic and Western North Pacific basins, ~55 and ~45 %, respectively, reintensify (not shown), consistent with Hart and Evans (2001). These results are not significantly different when reintensification is defined using 925-hPa wind speed (not shown). Globally, PRIMAVERA models generally overestimate climatological reintensification frequency at low resolution, but increasing resolution decreases the proportion of reintensifying systems (and increases the proportion of non-reintensifying systems) in all models except MPI-ESM1.2, which better matches reanalyses (Fig. 12b and Fig. 13b). This result potentially reflects improved simulation of the interactions between cyclones and the large-scale circulation, which acts to reintensify systems (Keller et al., 2019), at high resolution. Which processes facilitate such improvement should be a focus of future research because these processes will be important for risk assessments of reintensification. However, it is also possible that post-ET reintensification arises in models whose effective resolution increases with increasing latitude (e.g., HadGEM3-GC3.1), allowing stronger simulated winds at higher latitudes, but the impact of this artifact will be reduced at higher resolutions.

In HadGEM3-GC3.1, for an atmospheric resolution of 25 km (at 50 ° latitude), increasing ocean resolution from 1/4 ° to 1/12 ° (-HM and -HH, respectively) does not impact the proportion of reintensifying cyclones (Fig. 13b). An increase in the proportion might be expected because increasing ocean resolution and therefore more sharply resolving SST fronts (around western boundary currents; Fig. S5) is likely to enhance baroclinicity and provide atmospheric conditions conducive to post-ET reintensification. That no increase is seen implies that atmospheric resolution, to which simulated tropical-cyclone frequency and intensity are sensitive, acts as a constraint on reintensification statistics, at least for this particular model. Further investigation with multiple ocean models would establish more robustly whether this is the case.

In both the atmosphere-only and fully coupled simulations, future changes in the proportion of post-ET reintensifying systems are small and generally within one standard deviation of historical interannual variability (Fig. 12c and Fig. 13c), again suggesting that any climate-change response under RCP8.5 emerges after 2050. In atmosphere-only simulations, low-resolution models all simulate an increase the proportion of reintensifying cyclones, but high-resolution models simulate a decrease (Fig. 12c), except for CNRM-CM6.1. Fully coupled models typically simulate a future increase across resolutions (Fig. 13c).

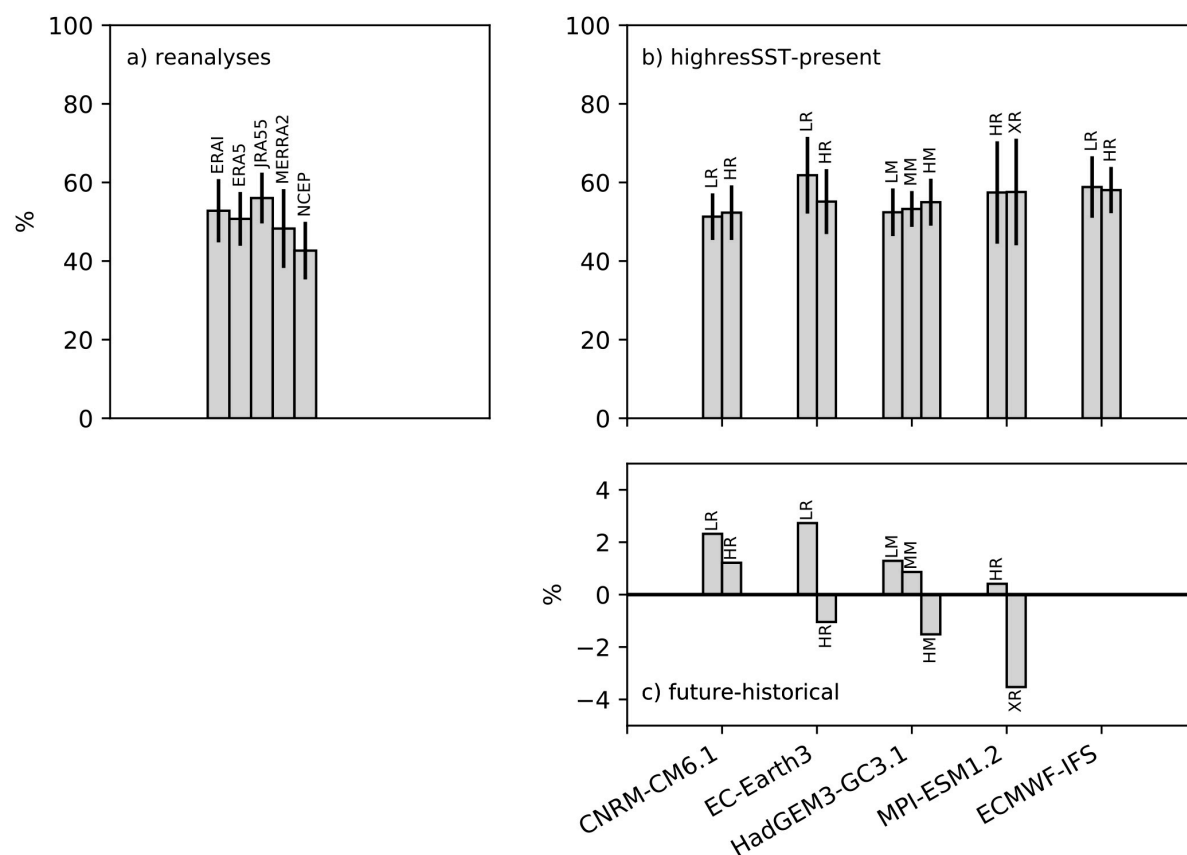


Fig. 12. Global analysis of the percentage of transitioning storms that undergo post-ET reintensification in (a) reanalyses and (b) *highresSST-present* simulations, and (c) the percentage change simulated for *highresSST-future* experiments. One standard deviation of interannual variability is indicated for each reanalysis and historical model simulation (black lines).

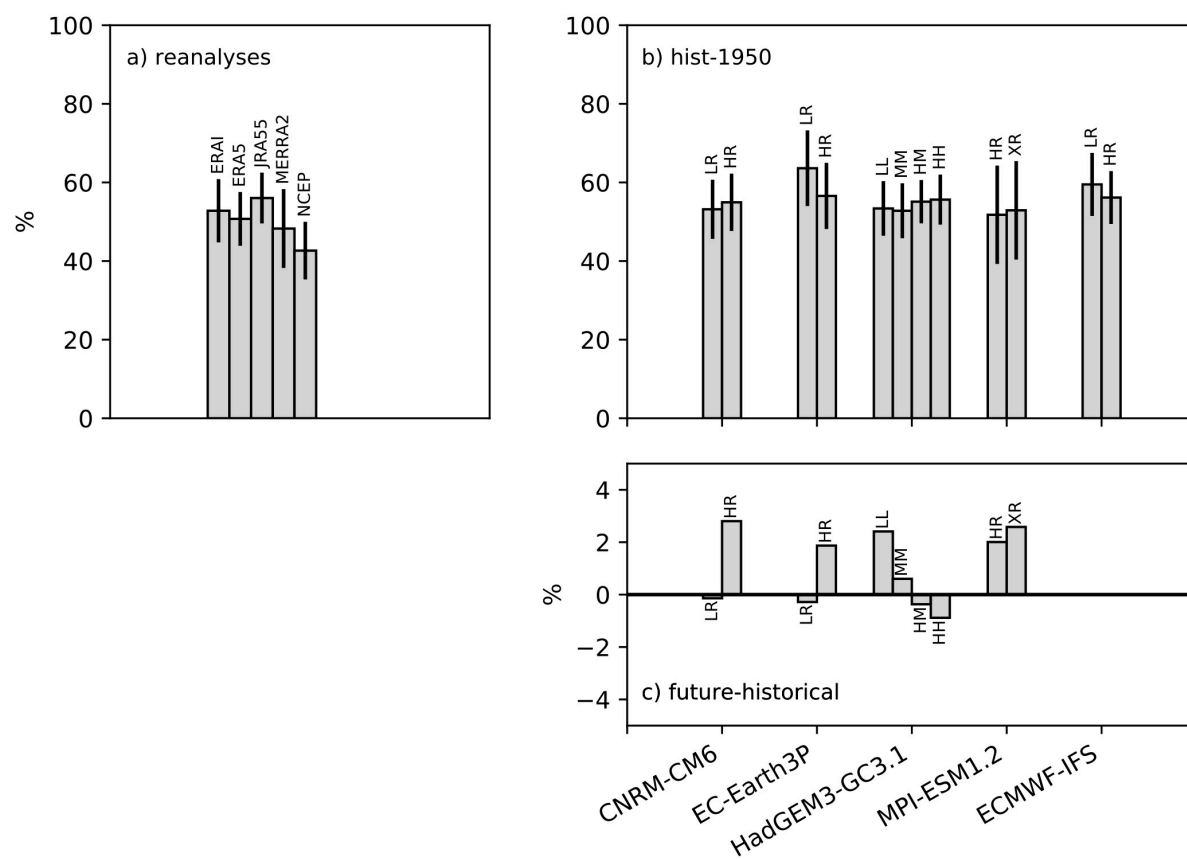


Fig. 13. As Fig. 12 but for *hist-1950* and *highres-future* simulations.

3.7 ET latitude

Finally, we assess how ET location responds to both increased resolution and to climate change out to 2050. Distributions of ET-completion latitude were computed from reanalyses and all PRIMAVERA experiments globally as well as separately for the basins where models exhibit the best performance: the North Atlantic and Western North Pacific basins (Fig. 14). For *highresSST-present*, model-simulated ET completion occurs at lower latitudes than in reanalyses (Fig. 14a–c). At high resolution, this is partially rectified: peak frequency occurs at a similar latitude to reanalyses in both the North Atlantic (Fig. 14a) and Western North Pacific (Fig. 14b), but the magnitudes of both peaks are underestimated and occurrences of low-latitude ET (i.e., 10–20 °) remain too frequent. Globally, an equatorward bias in peak frequency across resolutions indicates that ET-completion latitude is less well simulated in other basins (Fig. 14c). These results hold true for *hist-1950* simulations (Fig. 14d–f), except there are fewer instances of low-latitude ET (i.e., 10–20 °), likely reflecting slower development of warm-core structures and subsequent ET in the fully coupled experiments.

In response to climate change, the ensemble-mean distribution of ET-completion latitude exhibits an equatorward shift in the North Atlantic in the atmosphere-only experiment (Fig. 14a), but a poleward shift in the fully coupled simulations (Fig. 14d), with an increased frequency of ET completion particularly between 45–55 °N. In the Western North Pacific, a poleward shift is seen in the latitude of the peak frequency, from ~30 to ~40 °N, in both experiments, but little change is simulated at higher latitudes (i.e., > 45 °N). Globally, a small equatorward shift of ~2 ° is simulated in atmosphere-only (Fig. 14c) and no meridional shift is seen in coupled simulations (Fig. 14f). Previously, we showed stronger low-level warm-core structures are simulated in future (Fig. 6 and Fig. 8), which potentially allow tropical cyclones to propagate farther poleward prior to ET, with the most pronounced signal seen in the North Atlantic. While coupled PRIMAVERA models provide evidence for a poleward shift of ET, climate-change responses globally are equivocal out to 2050.

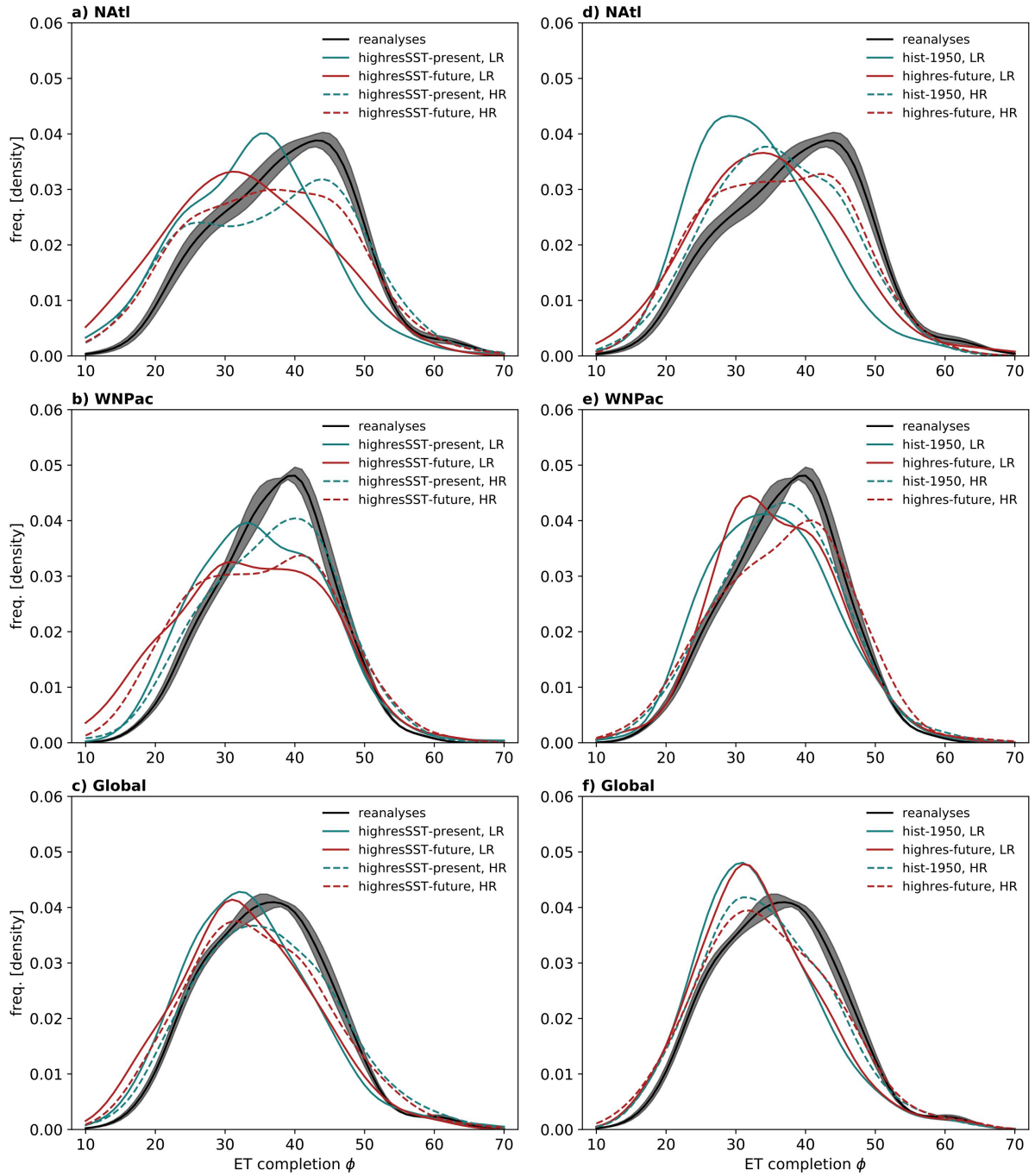


Fig. 14. Ensemble-mean frequency distributions of ET-completion latitude for (solid lines) low- and (dashed lines) high-resolution simulations, for both 1950–2014 (teal) and 2015–2050 (red). Results are shown for (a–c) atmosphere-only and (d–f) fully coupled experiments for the North Atlantic basin (“NAtl”), Western North Pacific basin (“WNPac”) and all global basins combined. ‘LR’ and ‘HR’ denote low- and high-resolution distributions, respectively. Also shown is the multireanalysis-mean distribution with shading indicating the standard error for the five reanalyses. Note that frequency is plotted as a function of absolute latitude (ϕ) to combine Northern and Southern Hemisphere results in c) and f).

4. Summary and discussion

This paper presents an analysis of ET across five reanalysis datasets and climate simulations performed with five atmosphere-only and full coupled global models participating in CMIP6 HighResMIP, focussing on (i) the effect of increased model resolution on the representation of ET and (ii) the response of ET to climate change.

For all tropical cyclones undergoing ET, we find an increase in the climatological track density simulated at high resolution (~25 km) compared with low resolution (~100 km) in all ocean basins and in both atmosphere-only and fully coupled model configurations (Fig. 1b, d), particularly over Northern Hemisphere western boundary currents. Model error in simulated track density (compared with the multireanalysis-mean track density) is reduced at high resolution in the North Atlantic and Western North Pacific (Fig. 1c, e). The simulated climatological annual-mean count of ET events is closer to that of reanalyses in the ocean basins where ET activity is highest—the North Atlantic and the Western and Eastern North Pacific—in both atmosphere-only (Fig. 3) and fully coupled (Fig. 4) experiments. In these basins, atmosphere-only simulations exhibit skill of ~0.3 in capturing interannual variability in just the subset of tropical cyclones that undergo ET (Table 4), demonstrating that the skill of these models in simulating all tropical cyclones does not remain throughout the complete cyclone lifecycle. Additionally, this level of skill in atmosphere-only simulations is lower than that found for similar-resolution initialised seasonal forecasts (Liu et al., 2018). For the other basins—the Northern Indian and Southern Hemisphere—frequencies simulated by high-resolution models overestimate reanalyses. ET %, however, is similar between low- and high-resolution simulations, indicating that the resolution sensitivity of ET is driven by that of tropical cyclone frequency, not by an enhancement of environmental conditions conducive to ET. The seasonal cycle of ET is reproduced by most models, with both the seasonal timing and the magnitude of the seasonal peak simulated more correctly at high-resolution, but the impact of increased atmospheric resolution is model-dependent.

In general, PRIMAVERA models show clearer inter-model agreement on the climate-change response of ET frequency than on the response of intensity-related metrics. For most basins, models simulate a frequency decrease in response to climate change, except over the North Atlantic, where an increase is projected (Fig. 2). The magnitude of the North Atlantic response is larger in atmosphere-only simulations than in fully coupled integrations and is

enhanced by increasing atmospheric model resolution, although interannual variability is pronounced (Fig. 3 and Fig. 4). A significant positive trend in the ensemble-mean fraction of North Atlantic ET events occurring during August–November is found over the period 1950–2050 at high-resolution, indicating long-term change in ET seasonality in this basin, but no secular seasonality change is simulated in the Western North Pacific (Fig. 5). North Atlantic seasonality change may result in a higher proportion of tropical cyclones encountering the midlatitude environment during the part of the seasonal cycle when, climatologically, baroclinicity is highest (Hoskins and Hodges, 2019). Opposing future ET responses between the North Atlantic and Western North Pacific are potentially underpinned by changes in low-level, pre-ET warm-core structures, which strengthen in response to climate change in the North Atlantic but undergo little change in the Western North Pacific (Fig. 6 and Fig. 7). Comparing atmosphere-only with fully coupled simulations, the North Atlantic track density response to climate change is more muted in the fully coupled experiment, which is consistent with a less pronounced climate-change response of pre-ET structures simulated by coupled models. Simulations with higher-resolution, storm-resolving models will open opportunities to further study realistically deep warm-core cyclones.

Globally, simulated warm-core, pre-ET intensity distributions improve with resolution in most models in both atmosphere-only and fully coupled experiments, better resembling reanalyses (Fig. 10 and Fig. 11). Simulated cold-core, post-ET intensity distributions exhibit little sensitivity to resolution across models. Globally, models simulate no clear climate-change response of pre- or post-ET intensity distributions, suggesting that, if a signal exists, extending simulations beyond 2050 may be required. Under *highresSST-future* forcing, some models show decreasing warm-core and increasing cold-core intensities for storms $<17\text{ms}^{-1}$, but the opposite response for storms $\geq 17\text{ms}^{-1}$. However, this is not reproduced by fully coupled models. Globally, increasing resolution increases the proportion of simulated post-ET reintensifications to approximately match reanalyses, but not in all models. Climate-change responses are not significant with respect to historical interannual variability and are model-dependent (Fig. 12 and Fig. 13).

The role of model resolution is become clearer, but uncertainties remain. Recent analysis of tropical cyclones the PRIMAVERA simulations (Roberts et al., 2020b) has shown that the high-resolution atmosphere-only models, which typically have lower wind-speed biases, show either reduced future wind speeds or no change. Fully coupled models with the smallest

historical biases simulate either no change in future wind speeds or increases of only a few percent. These models therefore project weaker intensity responses to climate change compared with other studies (Knutson et al., 2020). One potential factor is the simplifying aspects of the HighResMIP protocol that are necessary to isolate the role of model resolution, particularly the standardised aerosol forcing and use of a single set of SST and sea-ice boundary conditions shared across models (Haarsma et al., 2016). For ET, the climate-change responses of pre- and post-ET intensity analysed in this study are largely model-dependent, with models exhibiting little systematic change between atmospheric resolutions of ~ 100 and ~ 25 km. This suggests that these disparate responses are due to differences in model formulation, but a larger ensemble of models is likely needed to assess this fully. For post-ET reintensification, increasing atmospheric resolution appears to result in more consistent model behaviour, but resolution remains a key research issue because several models still underestimate tropical cyclone intensities at ~ 25 km grid spacing (Roberts et al., 2020a) and further improvements are anticipated by increasing resolution to at least 10 km (Haarsma, 2021; Judt et al., 2021). To obtain samples of ET events comparable to this study, however, running sufficiently long simulations (and / or a sufficiently large ensemble) at these storm-resolving resolutions, even without coupling to an ocean model, remains a significant computational challenge (Roberts et al., 2020b).

Additional outstanding questions and uncertainties remain. A poleward expansion of Hadley circulation termini is projected in a warmer climate (Lu et al., 2007), which implies meridional shifts in tropical storm tracks (Sharmila and Walsh, 2018; Studholme and Gulev, 2018). However, the impacts of this large-scale change on the spatial distribution and frequency of ET are equivocal. The poleward expansion of regions conducive to tropical cyclone genesis and development that results from an increase in Hadley cell width will reduce the mean displacement required for tropical cyclones to reach the midlatitude baroclinic zone, increasing the likelihood of ET. However, a poleward shift of the midlatitude storm track in response to warming has been projected (Bengtsson et al., 2006), which in turn shifts environmental conditions conducive to extratropical transition poleward, potentially offsetting Hadley-driven changes. Here, we find minimal changes in ET-completion latitude out to 2050 (Fig. 14), suggesting cancellation in the net effect of these competing large-scale changes. Further work is needed to establish the time of emergence of any meridional shift and will require dedicated studies, exploring a range of climate-change scenarios with models

run at resolutions sufficiently high to adequately represent both tropical cyclones and ET—at least 25 km, according to our results.

This study provides evidence that pre-ET cyclone intensity and warm-core strength exert influence over future changes in ET statistics and seasonality. Analysis of higher-resolution and storm-resolving models (at least 10 km) will help establish whether these results hold true for models able to reproduce more realistic tropical-cyclone maximum intensities, including rapidly intensifying systems. Additionally, there is a need to contextualise future projections of ET, accounting for natural variability, and in particular the roles of regional (e.g., Atlantic Multidecadal Variability) and global (i.e., El Niño–Southern Oscillation) modes of variability on ET frequency. Dedicated sensitivity experiments will be required, and such a study is forthcoming for the North Atlantic, where this work has identified future changes that are important and often unique to this basin. Finally, investigation of secular change in ET seasonality, as seen in the North Atlantic in this study, will be important globally because future modification to the interval between the seasonal maximum of ET occurrence and wintertime storminess may engender considerable changes in risk for populous midlatitude regions.

Data and code availability

All reanalysis data for tropical-cyclone tracking (vorticity, wind fields, and sea-level pressure) and cyclone phase-space analysis (geopotential) are available from rda.ucar.edu or disc.gsfc.nasa.gov. Model data are available from Earth System Grid Foundation nodes (esgf.llnl.gov). TRACK is available for download at gitlab.act.reading.ac.uk/track and the track datasets used in this paper may be downloaded from catalogue.ceda.ac.uk/uuid/e82a62d926d7448696a2b60c1925f811. Data analysis and visualisation code is available from the lead author upon request (hrcm.ceda.ac.uk/contact).

Acknowledgements

All authors received financial support from the PRIMAVERA project (European Commission Horizon2020 grant agreement 641727) with data access via JASMIN (jasmin.ac.uk) supported by IS-ENES3 (grant agreement 824084). AJB also received support from National Environmental Research Council (NERC) national capability grant for the North Atlantic Climate System: Integrated study (ACSIS) program (grants NE/N018001/1, NE/N018044/1, NE/N018028/1, and NE/N018052/1). KL received funding from the German Federal Ministry of Education and Research (BMBF) through JPI Climate / JPI Oceans NextG-Climate Science-ROADMAP (FKZ: 01LP2002A). The authors are grateful to the editor and to three anonymous reviewers, whose recommendations improved this paper.

Author contributions

AJB, PLV, RJH and MJR conceived the study. Simulations were performed by MJR, ET, KL, CDR, and LT. Output data were managed by JS. MJR performed the cyclone tracking. BV computed Eady growth rate. AJB undertook cyclone phase-space analysis and all other data analyses, figure preparation, and wrote the manuscript. All authors provided input in interpreting results and approved the final manuscript.

Competing interests

The authors declare no competing interests.

References

- Arnott, J. M., J. L. Evans, and F. Chiaromonte, 2004: Characterization of Extratropical Transition Using Cluster Analysis. *Monthly Weather Review* **132**, 2916-2937
- Baatsen, M., R. J. Haarsma, A. J. Van Delden, and H. de Vries, 2015: Severe Autumn storms in future Western Europe with a warmer Atlantic Ocean. *Climate Dynamics* **45**, 949-964
- Baker, A. J., K. I. Hodges, R. K. H. Schiemann, and P. L. Vidale, 2021: Historical variability and lifecycles of North Atlantic midlatitude cyclones originating in the tropics. *Journal of Geophysical Research: Atmospheres* **126**, e2020JD033924
- Balaguru, K., S. Taraphdar, L. R. Leung, G. R. Foltz, and J. A. Knaff, 2014: Cyclone-cyclone interactions through the ocean pathway. *Geophysical Research Letters* **41**, 6855-6862
- Barcikowska, M., F. Feser, and H. von Storch, 2012: Usability of Best Track Data in Climate Statistics in the Western North Pacific. *Monthly Weather Review* **140**, 2818-2830
- Bengtsson, L., K. I. Hodges, and E. Roeckner, 2006: Storm Tracks and Climate Change. *Journal of Climate* **19**, 3518-3543
- Bieli, M., S. J. Camargo, A. H. Sobel, J. L. Evans, and T. Hall, 2019: A Global Climatology of Extratropical Transition. Part I: Characteristics across Basins. *Journal of Climate* **32**, 3557-3582
- Bieli, M., A. H. Sobel, S. J. Camargo, H. Murakami, and G. A. Vecchi, 2020: Application of the Cyclone Phase Space to Extratropical Transition in a Global Climate Model. *Journal of Advances in Modeling Earth Systems* **12**, e2019MS001878
- Blake, E. S., T. B. Kimberlain, R. J. Berg, C. J.P., and J. L. Beven II, 2013: Hurricane Sandy (AL182012). *National Hurricane Center Tropical Cyclone Report*, https://www.nhc.noaa.gov/data/tcr/AL182012_Sandy.pdf
- Chang, E. K. M., and Y. Guo, 2007: Is the number of North Atlantic tropical cyclones significantly underestimated prior to the availability of satellite observations? *Geophysical Research Letters* **34**, L14801

1011 Chu, J.-H., C. R. Sampson, A. S. Levine, and E. Fukada, 2002: The Joint Typhoon Warning
1012 Center Tropical Cyclone Best-Tracks, 1945-2000. United States Naval Research Laboratory,
1013 NRL/MR/7540-02-16.

1014 Davis, C. A., 2018: Resolving Tropical Cyclone Intensity in Models. *Geophysical Research*
1015 *Letters* **45**, 2082-2087

1016 Dee, D. P., S. M. Uppala, A. J. Simmons, P. Berrisford, P. Poli, S. Kobayashi, U. Andrae, M.
1017 A. Balmaseda, G. Balsamo, P. Bauer, P. Bechtold, A. C. M. Beljaars, L. van de Berg, J.
1018 Bidlot, N. Bormann, C. Delsol, R. Dragani, M. Fuentes, A. J. Geer, L. Haimberger, S. B.
1019 Healy, H. Hersbach, E. V. Hólm, L. Isaksen, P. Kållberg, M. Köhler, M. Matricardi, A. P.
1020 McNally, B. M. Monge-Sanz, J. J. Morcrette, B. K. Park, C. Peubey, P. de Rosnay, C.
1021 Tavolato, J. N. Thépaut, and F. Vitart, 2011: The ERA-Interim reanalysis: configuration and
1022 performance of the data assimilation system. *Quarterly Journal of the Royal Meteorological*
1023 *Society* **137**, 553-597

1024 Dekker, M. M., R. J. Haarsma, H. d. Vries, M. Baatsen, and A. J. v. Delden, 2018:
1025 Characteristics and development of European cyclones with tropical origin in reanalysis data.
1026 *Climate Dynamics* **50**, 445-455

1027 Delgado, S., C. W. Landsea, and H. Willoughby, 2018: Reanalysis of the 1954–63 Atlantic
1028 Hurricane Seasons. *Journal of Climate* **31**, 4177-4192

1029 Evans, C., K. M. Wood, S. D. Aberson, H. M. Archambault, S. M. Milrad, L. F. Bosart, K. L.
1030 Corbosiero, C. A. Davis, J. R. D. Pinto, J. Doyle, C. Fogarty, T. J. G. Jr., C. M. Grams, K. S.
1031 Griffin, J. Gyakum, R. E. Hart, N. Kitabatake, H. S. Lentink, R. McTaggart-Cowan, W.
1032 Perrie, J. F. D. Quinting, C. A. Reynolds, M. Riemer, E. A. Ritchie, Y. Sun, and F. Zhang,
1033 2017: The Extratropical Transition of Tropical Cyclones. Part I: Cyclone Evolution and
1034 Direct Impacts. *Monthly Weather Review* **145**, 4317-4344

1035 Grams, C. M., and S. R. Blumer, 2015: European high-impact weather caused by the
1036 downstream response to the extratropical transition of North Atlantic Hurricane Katia (2011).
1037 *Geophysical Research Letters* **42**, 8738-8748

1038 Gutjahr, O., D. Putrasahan, K. Lohmann, J. H. Jungclaus, J. S. von Storch, N. Brüggemann,
1039 H. Haak, and A. Stössel, 2019: Max Planck Institute Earth System Model (MPI-ESM1.2) for

1040 the High-Resolution Model Intercomparison Project (HighResMIP). *Geosci. Model Dev.* **12**,
1041 3241-3281

1042 Haarsma, R., 2021: European Windstorm Risk of Post-Tropical Cyclones and the Impact of
1043 Climate Change. *Geophysical Research Letters* **48**, e2020GL091483

1044 Haarsma, R., M. Acosta, R. Bakhshi, P. A. Bretonnière, L. P. Caron, M. Castrillo, S. Corti, P.
1045 Davini, E. Exarchou, F. Fabiano, U. Fladrich, R. Fuentes Franco, J. García-Serrano, J. von
1046 Hardenberg, T. Koenig, X. Levine, V. L. Meccia, T. van Noije, G. van den Oord, F. M.
1047 Palmeiro, M. Rodrigo, Y. Ruprich-Robert, P. Le Sager, E. Tourigny, S. Wang, M. van Weele,
1048 and K. Wyser, 2020: HighResMIP versions of EC-Earth: EC-Earth3P and EC-Earth3P-HR –
1049 description, model computational performance and basic validation. *Geosci. Model Dev.* **13**,
1050 3507-3527

1051 Haarsma, R. J., W. Hazeleger, C. Severijns, H. Vries, A. Sterl, R. Bintanja, G. J. Oldenborgh,
1052 and H. W. Brink, 2013: More hurricanes to hit western Europe due to global warming.
1053 *Geophysical Research Letters* **40**, 1783-1788

1054 Haarsma, R. J., M. J. Roberts, P. L. Vidale, C. A. Senior, A. Bellucci, Q. Bao, P. Chang, S.
1055 Corti, N. S. Fučkar, V. Guemas, J. von Hardenberg, W. Hazeleger, C. Kodama, T. Koenig,
1056 L. R. Leung, J. Lu, J. J. Luo, J. Mao, M. S. Mizieliński, R. Mizuta, P. Nobre, M. Satoh, E.
1057 Scoccimarro, T. Semmler, J. Small, and J. S. von Storch, 2016: High Resolution Model
1058 Intercomparison Project (HighResMIP v1.0) for CMIP6. *Geoscientific Model Development* **9**,
1059 4185-4208

1060 Hagen, A. B., D. Strahan-Sakoskie, and C. Luckett, 2012: A Reanalysis of the 1944–53
1061 Atlantic Hurricane Seasons—The First Decade of Aircraft Reconnaissance. *Journal of*
1062 *Climate* **25**, 4441-4460

1063 Harr, P. A., D. Anwender, and S. C. Jones, 2008: Predictability Associated with the
1064 Downstream Impacts of the Extratropical Transition of Tropical Cyclones: Methodology and
1065 a Case Study of Typhoon Nabi (2005). *Monthly Weather Review* **136**, 3205-3225

1066 Hart, R. E., 2003: A Cyclone Phase Space Derived from Thermal Wind and Thermal
1067 Asymmetry. *Monthly Weather Review* **131**, 585-616

1068 Hart, R. E., and J. L. Evans, 2001: A Climatology of the Extratropical Transition of Atlantic
1069 Tropical Cyclones. *Journal of Climate* **14**, 546-564

1070 Hart, R. E., J. L. Evans, and C. Evans, 2006: Synoptic Composites of the Extratropical
1071 Transition Life Cycle of North Atlantic Tropical Cyclones: Factors Determining
1072 Posttransition Evolution. *Monthly Weather Review* **134**, 553-578

1073 Hersbach, H., B. Bell, P. Berrisford, S. Hirahara, A. Horányi, J. Muñoz-Sabater, J. Nicolas,
1074 C. Peubey, R. Radu, D. Schepers, A. Simmons, C. Soci, S. Abdalla, X. Abellan, G. Balsamo,
1075 P. Bechtold, G. Biavati, J. Bidlot, M. Bonavita, G. De Chiara, P. Dahlgren, D. Dee, M.
1076 Diamantakis, R. Dragani, J. Flemming, R. Forbes, M. Fuentes, A. Geer, L. Haimberger, S.
1077 Healy, R. J. Hogan, E. Hólm, M. Janisková, S. Keeley, P. Laloyaux, P. Lopez, C. Lupu, G.
1078 Radnoti, P. de Rosnay, I. Rozum, F. Vamborg, S. Villaume, and J.-N. Thépaut, 2020: The
1079 ERA5 global reanalysis. *Quarterly Journal of the Royal Meteorological Society* **146**, 1999-
1080 2049

1081 Hodges, K. I., 1995: Feature Tracking on the Unit Sphere. *Monthly Weather Review* **123**,
1082 3458-3465

1083 Hodges, K. I., 1996: Spherical Nonparametric Estimators Applied to the UGAMP Model
1084 Integration for AMIP. *Monthly Weather Review* **124**, 2914-2932

1085 Hodges, K. I., 1999: Adaptive Constraints for Feature Tracking. *Monthly Weather Review*
1086 **127**, 1362-1373

1087 Hodges, K. I., A. Cobb, and P. L. Vidale, 2017: How Well Are Tropical Cyclones
1088 Represented in Reanalysis Datasets? *Journal of Climate* **30**, 5243-5264

1089 Hoskins, B. J., and K. I. Hodges, 2019: The Annual Cycle of Northern Hemisphere Storm
1090 Tracks. Part I: Seasons. *Journal of Climate* **32**, 1743-1760

1091 Hoskins, B. J., and P. J. Valdes, 1990: On the Existence of Storm-Tracks. *Journal of the*
1092 *Atmospheric Sciences* **47**, 1854-1864

1093 Ito, R., T. Takemi, and O. Arakawa, 2016: A Possible Reduction in the Severity of Typhoon
1094 Wind in the Northern Part of Japan under Global Warming: A Case Study. *SOLA* **12**, 100-105

1095 Jones, S. C., P. A. Harr, J. Abraham, L. F. Bosart, P. J. Bowyer, J. L. Evans, D. E. Hanley, B.
 1096 N. Hanstrum, R. E. Hart, F. Lalaurette, M. R. Sinclair, R. K. Smith, and C. Thorncroft, 2003:
 1097 The Extratropical Transition of Tropical Cyclones: Forecast Challenges, Current
 1098 Understanding, and Future Directions. *Weather and Forecasting* **18**, 1052-1092

1099 Judt, F., D. Klocke, R. Rios-Berrios, B. Vannière, F. Ziemer, L. Auger, J. Biercamp, C.
 1100 Bretherton, X. Chen, P. Düben, C. Hohenegger, M. Khairoutdinov, C. Kodama, L.
 1101 Kornblueh, S.-J. Lin, M. Nakano, P. Neumann, W. Putman, N. Röber, M. Roberts, M. Satoh,
 1102 R. Shibuya, B. Stevens, P. L. Vidale, N. Wedi, and L. Zhou, 2021: Tropical Cyclones in
 1103 Global Storm-Resolving Models. *Journal of the Meteorological Society of Japan. Ser. II* **99**,
 1104 579-602

1105 Jung, C., and G. M. Lackmann, 2021: The Response of Extratropical Transition of Tropical
 1106 Cyclones to Climate Change: Quasi-Idealized Numerical Experiments. *Journal of Climate*
 1107 **34**, 4361-4381

1108 Keller, J. H., C. M. Grams, M. Riemer, H. M. Archambault, L. Bosart, J. D. Doyle, J. L.
 1109 Evans, T. J. G. Jr., K. Griffin, P. A. Harr, N. Kitabatake, R. McTaggart-Cowan, F. Pantillon,
 1110 J. F. Quinting, C. A. Reynolds, E. A. Ritchie, R. D. Torn, and F. Zhang, 2019: The
 1111 Extratropical Transition of Tropical Cyclones. Part II: Interaction with the Midlatitude Flow,
 1112 Downstream Impacts, and Implications for Predictability. *Monthly Weather Review* **147**,
 1113 1077-1106

1114 Kitabatake, N., 2011: Climatology of Extratropical Transition of Tropical Cyclones in the
 1115 Western North Pacific Defined by Using Cyclone Phase Space. *Journal of the*
 1116 *Meteorological Society of Japan. Ser. II* **89**, 309-325

1117 Klaver, R., R. Haarsma, P. L. Vidale, and W. Hazeleger, 2020: Effective resolution in high
 1118 resolution global atmospheric models for climate studies. *Atmospheric Science Letters* **21**,
 1119 e952

1120 Klein, P. M., P. A. Harr, and R. L. Elsberry, 2002: Extratropical Transition of Western North
 1121 Pacific Tropical Cyclones: Midlatitude and Tropical Cyclone Contributions to
 1122 Reintensification. *Monthly Weather Review* **130**, 2240-2259

- 1123 Knutson, T., S. J. Camargo, J. C. L. Chan, K. Emanuel, C.-H. Ho, J. Kossin, M. Mohapatra,
 1124 M. Satoh, M. Sugi, K. Walsh, and L. Wu, 2020: Tropical Cyclones and Climate Change
 1125 Assessment: Part II: Projected Response to Anthropogenic Warming. *Bulletin of the*
 1126 *American Meteorological Society* **101**, E303-E322
- 1127 Kobayashi, S., Y. Ota, Y. Harada, A. Ebita, M. Moriya, H. Onoda, K. Onogi, H. Kamahori,
 1128 C. Kobayashi, H. Endo, K. Miyaoka, and K. Takahashi, 2015: The JRA-55 Reanalysis:
 1129 General Specifications and Basic Characteristics. *Journal of the Meteorological Society of*
 1130 *Japan. Ser. II* **93**, 5-48
- 1131 Kofron, D. E., E. A. Ritchie, and J. S. Tyo, 2010: Determination of a Consistent Time for the
 1132 Extratropical Transition of Tropical Cyclones. Part I: Examination of Existing Methods for
 1133 Finding “ET Time”. *Monthly Weather Review* **138**, 4328-4343
- 1134 Kossin, J. P., K. R. Knapp, D. J. Vimont, R. J. Murnane, and B. A. Harper, 2007: A globally
 1135 consistent reanalysis of hurricane variability and trends. *Geophysical Research Letters* **34**
- 1136 Lanzante, J. R., 2019: Uncertainties in tropical-cyclone translation speed. *Nature* **570**, E6-
 1137 E15
- 1138 Laurila, T. K., V. A. Sinclair, and H. Gregow, 2019: The Extratropical Transition of
 1139 Hurricane Debby (1982) and the Subsequent Development of an Intense Windstorm over
 1140 Finland. *Monthly Weather Review* **148**, 377-401
- 1141 Liu, M., G. A. Vecchi, J. A. Smith, and H. Murakami, 2017: The Present-Day Simulation and
 1142 Twenty-First-Century Projection of the Climatology of Extratropical Transition in the North
 1143 Atlantic. *Journal of Climate* **30**, 2739-2756
- 1144 Liu, M., G. A. Vecchi, J. A. Smith, H. Murakami, R. Gudgel, and X. Yang, 2018: Towards
 1145 Dynamical Seasonal Forecast of Extratropical Transition in the North Atlantic. *Geophysical*
 1146 *Research Letters* **45**, 12,602-612,609
- 1147 Lu, J., G. A. Vecchi, and T. Reichler, 2007: Expansion of the Hadley cell under global
 1148 warming. *Geophysical Research Letters* **34**

1149 Manganello, J. V., B. A. Cash, K. I. Hodges, and J. L. Kinter, 2019: Seasonal forecasts of
 1150 North Atlantic tropical cyclone activity in the North American Multi-Model Ensemble.
 1151 *Climate Dynamics* **53**, 7169-7184

1152 Michaelis, A. C., and G. M. Lackmann, 2019: Climatological Changes in the Extratropical
 1153 Transition of Tropical Cyclones in High-Resolution Global Simulations. *Journal of Climate*
 1154 **32**, 8733-8753

1155 Michaelis, A. C., and G. M. Lackmann, 2021: Storm-Scale Dynamical Changes of
 1156 Extratropical Transition Events in Present-Day and Future High-Resolution Global
 1157 Simulations. *Journal of Climate* **34**, 5037-5062

1158 Molod, A., L. Takacs, M. Suarez, and J. Bacmeister, 2015: Development of the GEOS-5
 1159 atmospheric general circulation model: evolution from MERRA to MERRA2. *Geosci. Model*
 1160 *Dev.* **8**, 1339-1356

1161 Moon, I.-J., S.-H. Kim, and J. C. L. Chan, 2019: Climate change and tropical cyclone trend.
 1162 *Nature* **570**, E3-E5

1163 Moreno-Chamarro, E., L. P. Caron, S. Loosveldt Tomas, J. Vegas-Regidor, O. Gutjahr, M. P.
 1164 Moine, D. Putrasahan, C. D. Roberts, M. J. Roberts, R. Senan, L. Terray, E. Tourigny, and P.
 1165 L. Vidale, 2022: Impact of increased resolution on long-standing biases in HighResMIP-
 1166 PRIMAVERA climate models. *Geosci. Model Dev.* **15**, 269-289

1167 Murakami, H., 2014: Tropical cyclones in reanalysis data sets. *Geophysical Research Letters*
 1168 **41**, 2133-2141

1169 Rantanen, M., J. Räisänen, V. A. Sinclair, J. Lento, and H. Järvinen, 2020: The extratropical
 1170 transition of Hurricane Ophelia (2017) as diagnosed with a generalized omega equation and
 1171 vorticity equation. *Tellus A: Dynamic Meteorology and Oceanography* **72**, 1-26

1172 Roberts, C. D., R. Senan, F. Molteni, S. Boussetta, M. Mayer, and S. P. E. Keeley, 2018:
 1173 Climate model configurations of the ECMWF Integrated Forecasting System (ECMWF-IFS
 1174 cycle 43r1) for HighResMIP. *Geosci. Model Dev.* **11**, 3681-3712

1175 Roberts, M. J., A. Baker, E. W. Blockley, D. Calvert, A. Coward, H. T. Hewitt, L. C.
 1176 Jackson, T. Kuhlbrodt, P. Mathiot, C. D. Roberts, R. Schiemann, J. Seddon, B. Vannière, and

1177 P. L. Vidale, 2019: Description of the resolution hierarchy of the global coupled HadGEM3-
 1178 GC3.1 model as used in CMIP6 HighResMIP experiments. *Geosci. Model Dev.* **12**, 4999-
 1179 5028

1180 Roberts, M. J., J. Camp, J. Seddon, P. L. Vidale, K. Hodges, B. Vanniere, J. Mecking, R.
 1181 Haarsma, A. Bellucci, E. Scoccimarro, L.-P. Caron, F. Chauvin, L. Terray, S. Valcke, M.-P.
 1182 Moine, D. Putrasahan, C. Roberts, R. Senan, C. Zarzycki, and P. Ullrich, 2020a: Impact of
 1183 Model Resolution on Tropical Cyclone Simulation Using the HighResMIP-PRIMAVERA
 1184 Multimodel Ensemble. *Journal of Climate* **33**, 2557-2583

1185 Roberts, M. J., J. Camp, J. Seddon, P. L. Vidale, K. Hodges, B. Vannière, J. Mecking, R.
 1186 Haarsma, A. Bellucci, E. Scoccimarro, L.-P. Caron, F. Chauvin, L. Terray, S. Valcke, M.-P.
 1187 Moine, D. Putrasahan, C. D. Roberts, R. Senan, C. Zarzycki, P. Ullrich, Y. Yamada, R.
 1188 Mizuta, C. Kodama, D. Fu, Q. Zhang, G. Danabasoglu, N. Rosenbloom, H. Wang, and L.
 1189 Wu, 2020b: Projected Future Changes in Tropical Cyclones Using the CMIP6 HighResMIP
 1190 Multimodel Ensemble. *Geophysical Research Letters* **47**, e2020GL088662

1191 Roberts, M. J., P. L. Vidale, M. S. Mizieliński, M.-E. Demory, R. Schiemann, J. Strachan, K.
 1192 Hodges, R. Bell, and J. Camp, 2015: Tropical Cyclones in the UPSCALE Ensemble of High-
 1193 Resolution Global Climate Models. *Journal of Climate* **28**, 574-596

1194 Saha, S., S. Moorthi, X. Wu, J. Wang, S. Nadiga, P. Tripp, D. Behringer, Y.-T. Hou, H.-y.
 1195 Chuang, M. Iredell, M. Ek, J. Meng, R. Yang, M. P. Mendez, H. v. d. Dool, Q. Zhang, W.
 1196 Wang, M. Chen, and E. Becker, 2014: The NCEP Climate Forecast System Version 2.
 1197 *Journal of Climate* **27**, 2185-2208

1198 Sainsbury, E. M., R. K. H. Schiemann, K. I. Hodges, L. C. Shaffrey, A. J. Baker, and K. T.
 1199 Bhatia, 2020: How Important Are Post-Tropical Cyclones for European Windstorm Risk?
 1200 *Geophysical Research Letters* **47**, e2020GL089853

1201 Schreck III, C. J., K. R. Knapp, and J. P. Kossin, 2014: The Impact of Best Track
 1202 Discrepancies on Global Tropical Cyclone Climatologies using IBTrACS. *Monthly Weather*
 1203 *Review* **142**, 3881-3899

1204 Sharmila, S., and K. J. E. Walsh, 2018: Recent poleward shift of tropical cyclone formation
 1205 linked to Hadley cell expansion. *Nature Climate Change* **8**, 730-736

1206 Stewart, S. R., 2018: Hurricane Ophelia (AL172017). *National Hurricane Center Tropical*
1207 *Cyclone Report*, www.nhc.noaa.gov/data/tcr/AL172017_Ophelia.pdf

1208 Strachan, J., P. L. Vidale, K. Hodges, M. Roberts, and M.-E. Demory, 2013: Investigating
1209 Global Tropical Cyclone Activity with a Hierarchy of AGCMs: The Role of Model
1210 Resolution. *Journal of Climate* **26**, 133-152

1211 Studholme, J., A. V. Fedorov, S. K. Gulev, K. Emanuel, and K. Hodges, 2022: Poleward
1212 expansion of tropical cyclone latitudes in warming climates. *Nature Geoscience* **15**, 14-28

1213 Studholme, J., and S. Gulev, 2018: Concurrent Changes to Hadley Circulation and the
1214 Meridional Distribution of Tropical Cyclones. *Journal of Climate* **31**, 4367-4389

1215 Studholme, J., K. I. Hodges, and C. M. Brierley, 2015: Objective determination of the
1216 extratropical transition of tropical cyclones in the Northern Hemisphere. *Tellus A: Dynamic*
1217 *Meteorology and Oceanography* **67**, 24474

1218 Vanni re, B., M. Roberts, P. L. Vidale, K. Hodges, M.-E. Demory, L.-P. Caron, E.
1219 Scoccimarro, L. Terray, and R. Senan, 2020: The Moisture Budget of Tropical Cyclones in
1220 HighResMIP Models: Large-Scale Environmental Balance and Sensitivity to Horizontal
1221 Resolution. *Journal of Climate* **33**, 8457-8474

1222 Vecchi, G. A., T. L. Delworth, H. Murakami, S. D. Underwood, A. T. Wittenberg, F. Zeng,
1223 W. Zhang, J. W. Baldwin, K. T. Bhatia, W. Cooke, J. He, S. B. Kapnick, T. R. Knutson, G.
1224 Villarini, K. van der Wiel, W. Anderson, V. Balaji, J. H. Chen, K. W. Dixon, R. Gudgel, L.
1225 M. Harris, L. Jia, N. C. Johnson, S.-J. Lin, M. Liu, C. H. J. Ng, A. Rosati, J. A. Smith, and X.
1226 Yang, 2019: Tropical cyclone sensitivities to CO2 doubling: roles of atmospheric resolution,
1227 synoptic variability and background climate changes. *Climate Dynamics* **53**, 5999-6033

1228 Vecchi, G. A., and T. R. Knutson, 2008: On Estimates of Historical North Atlantic Tropical
1229 Cyclone Activity. *Journal of Climate* **21**, 3580-3600

1230 Vecchi, G. A., and T. R. Knutson, 2011: Estimating Annual Numbers of Atlantic Hurricanes
1231 Missing from the HURDAT Database (1878–1965) Using Ship Track Density. *Journal of*
1232 *Climate* **24**, 1736-1746

1233 Velden, C., B. Harper, F. Wells, J. L. Beven, R. Zehr, T. Olander, M. Mayfield, C. C. Guard,
 1234 M. Lander, R. Edson, L. Avila, A. Burton, M. Turk, A. Kikuchi, A. Christian, P. Caroff, and
 1235 P. McCrone, 2006: The Dvorak Tropical Cyclone Intensity Estimation Technique: A
 1236 Satellite-Based Method that Has Endured for over 30 Years. *Bulletin of the American*
 1237 *Meteorological Society* **87**, 1195-1210

1238 Vidale, P. L., K. Hodges, B. Vannière, P. Davini, M. J. Roberts, K. Strommen, A.
 1239 Weisheimer, E. Plesca, and S. Corti, 2021: Impact of Stochastic Physics and Model
 1240 Resolution on the Simulation of Tropical Cyclones in Climate GCMs. *Journal of Climate* **34**,
 1241 4315-4341

1242 Voldoire, A., D. Saint-Martin, S. Sénési, B. Decharme, A. Alias, M. Chevallier, J. Colin, J. F.
 1243 Guérémy, M. Michou, M. P. Moine, P. Nabat, R. Roehrig, D. Salas y Mélia, R. Sférian, S.
 1244 Valcke, I. Beau, S. Belamari, S. Berthet, C. Cassou, J. Cattiaux, J. Deshayes, H. Douville, C.
 1245 Ethé, L. Franchistéguy, O. Geoffroy, C. Lévy, G. Madec, Y. Meurdesoif, R. Msadek, A.
 1246 Ribes, E. Sanchez-Gomez, L. Terray, and R. Waldman, 2019: Evaluation of CMIP6 DECK
 1247 Experiments With CNRM-CM6-1. *Journal of Advances in Modeling Earth Systems* **11**, 2177-
 1248 2213

1249 Weinkle, J., C. Landsea, D. Collins, R. Musulin, R. P. Crompton, P. J. Klotzbach, and R.
 1250 Pielke, 2018: Normalized hurricane damage in the continental United States 1900–2017.
 1251 *Nature Sustainability* **1**, 808-813

1252 Williams, K. D., D. Copsey, E. W. Blockley, A. Bodas-Salcedo, D. Calvert, R. Comer, P.
 1253 Davis, T. Graham, H. T. Hewitt, R. Hill, P. Hyder, S. Ineson, T. C. Johns, A. B. Keen, R. W.
 1254 Lee, A. Megann, S. F. Milton, J. G. L. Rae, M. J. Roberts, A. A. Scaife, R. Schiemann, D.
 1255 Storkey, L. Thorpe, I. G. Watterson, D. N. Walters, A. West, R. A. Wood, T. Woollings, and
 1256 P. K. Xavier, 2018: The Met Office Global Coupled Model 3.0 and 3.1 (GC3.0 and GC3.1)
 1257 Configurations. *Journal of Advances in Modeling Earth Systems* **10**, 357-380

1258 Wood, K. M., and E. A. Ritchie, 2014: A 40-Year Climatology of Extratropical Transition in
 1259 the Eastern North Pacific. *Journal of Climate* **27**, 5999-6015

1260 Zarzycki, C. M., D. R. Thatcher, and C. Jablonowski, 2017: Objective tropical cyclone
 1261 extratropical transition detection in high-resolution reanalysis and climate model data.
 1262 *Journal of Advances in Modeling Earth Systems* **9**, 130-148

1263 Zhu, X., L. Wu, and Q. Wang, 2018: Extratropical Transition and Re-Intensification of
1264 Typhoon Toraji (2001): Large-Scale Circulations, Structural Characteristics, and Mechanism
1265 Analysis. *Journal of Ocean University of China* **17**, 461-476
1266

Supplementary information

Extratropical transition of tropical cyclones in a multiresolution ensemble of atmosphere-only and fully coupled global climate models

Alexander J. Baker^{1,*}, Malcolm J. Roberts², Pier Luigi Vidale¹, Kevin I. Hodges¹, Jon Seddon², Benoît Vannière¹, Rein J. Haarsma³, Reinhard Schiemann¹, Dimitris Kapetanakis³, Etienne Tourigny⁴, Katja Lohmann⁵, Christopher D. Roberts⁶, and Laurent Terray⁷

¹ National Centre for Atmospheric Science and Department of Meteorology, University of Reading, Reading, Berkshire, UK

² Met Office Hadley Centre, Exeter, Devon, UK

³ Koninklijk Nederlands Meteorologisch Instituut, De Bilt, The Netherlands

⁴ Earth Sciences Department, Barcelona Supercomputing Center, Barcelona, Spain

⁵ Max Planck Institut für Meteorologie, Hamburg, Germany

⁶ European Centre for Medium-Range Weather Forecasts (ECMWF), Reading, UK

⁷ Climat, Environnement, Couplages et Incertitudes, Centre Européen de Recherche et de Formation Avancée en Calcul Scientifique (CERFACS), Toulouse, France

* alexander.baker@reading.ac.uk

Corresponding author: Dr Alexander J. Baker

National Centre for Atmospheric Science

Department of Meteorology,

University of Reading

Earley Gate, Whiteknights Road, Reading, Berkshire RG6 6ES, UK

+44 (0) 118 377 762

S1. Methodological considerations

Two important methodological considerations in ET studies are discussed in this section: (i) the cyclone-tracking algorithm and (ii) the sensitivity of ET location to how ET is identified.

S1.1 Cyclone-tracking algorithm

Recent studies of tropical cyclones in reanalyses and simulated by climate models (e.g., Roberts et al., 2020a; Vannière et al., 2020) compared results obtained using TRACK with TempestExtremes, a sea-level-pressure-based tracking algorithm (Ullrich and Zarzycki, 2017), to show that, broadly, their results are robust to algorithm choice. However, tracks output by TempestExtremes represent only cyclones' warm-core stages, and as such few identified systems undergo ET (Fig. S1). Therefore, supplementary algorithms are required to extend cyclone tracks generated using TempestExtremes into the midlatitudes (e.g., Michaelis and Lackmann, 2019; Zarzycki et al., 2017), but the extent to which results are sensitive to the additional methodological choices necessary in this approach is unclear. In this study, use of TRACK, a vorticity-based algorithm that satisfactorily yields complete cyclone lifecycles based on a single set of identification criteria, is clearly advantageous in our analysis of ET statistics. Once comparable whole-lifecycle tracks, including post-tropical evolution, from multiple, independent algorithms are available, sensitivity analysis should be a research priority.

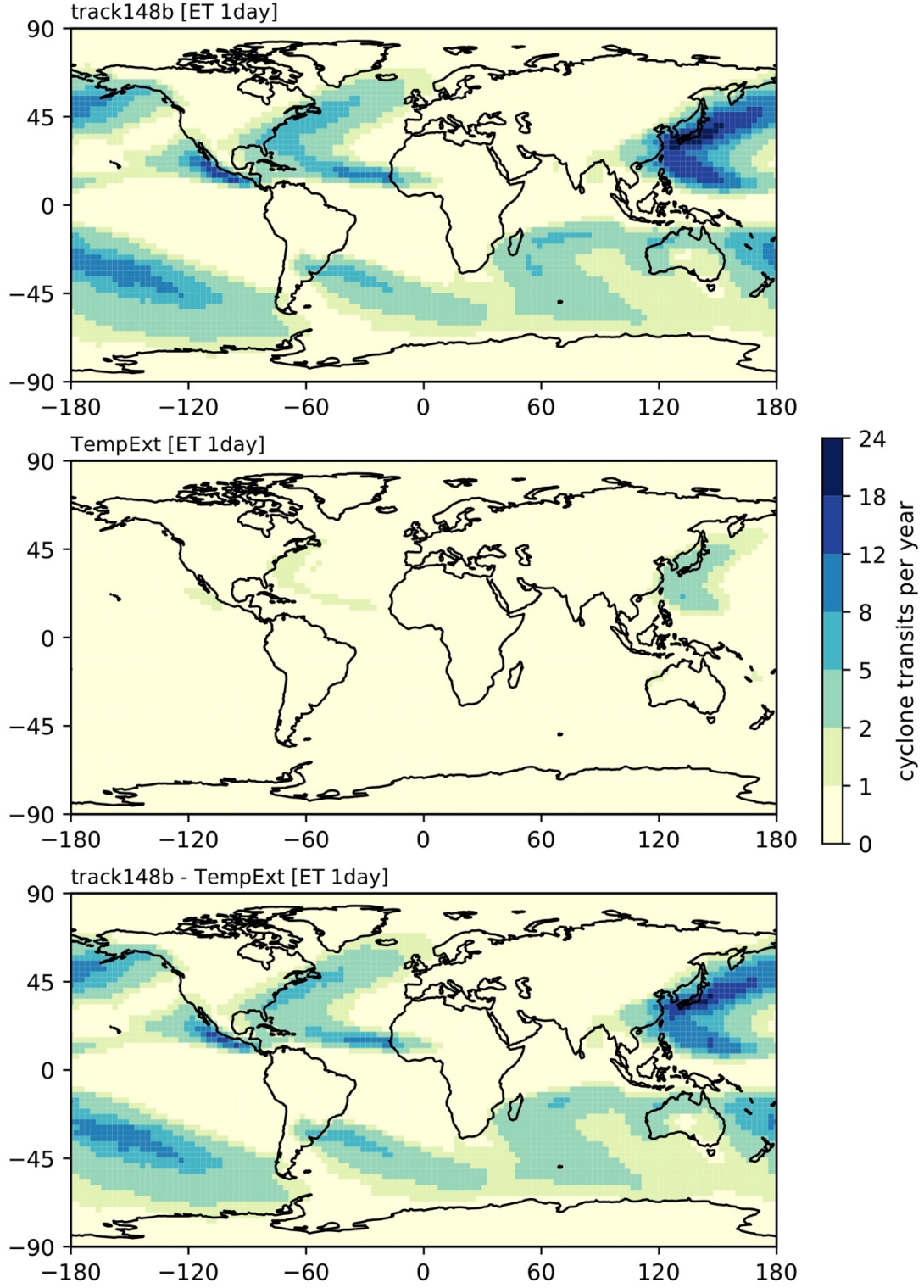


Fig. S1. Multi-reanalysis-mean track density in TCs undergoing ET identified by two feature-tracking algorithms: (top) TRACK (“track148b”) and (middle) TempestExtremes (“TempExt”). We also show (bottom) the inter-algorithm difference (i.e., TRACK minus TempestExtremes).

S1.2 Sensitivity of ET location to identification method

Recent analysis of ERA5 shows that phase-space-based identification of post-tropical structures compares well with other methods in terms of the number of ET events identified (Sainsbury et al., 2020) and phase-space methodologies are the most common across studies of ET. However, no consensus approach to identifying ET onset and completion based on phase-space parameters exists. Previous studies have applied differing absolute thresholds to identify changes in cyclone thermal symmetry and employed additional criteria, such as intensity thresholds and temporal smoothing of phase-space series. These modifications have little impact on the number of identified events, but the location of ET may be sensitive to how phase-space parameters are treated. We conducted an overview assessment of this in reanalyses by mapping the mean ET-completion locations for various identification approaches (Fig. S2). In the North Atlantic and Western North Pacific, a definition of ET where both ET onset and completion are identified by single-timestep B or T_L changes (‘conventional’) yields the lowest-latitude ET completion (Fig. S2). In contrast, applying a prior warm-core test, as in the previous section (4.2), yields ET completion in the range of 30–40 ° latitude, coinciding with the known centres of baroclinicity associated with western boundary currents. Other proposed modifications of ET identification—imposing a v_{max} threshold, applying a temporal smoothing, and requiring B and T_L criteria are met for consecutive timesteps—yield locations in between these two approaches, with greater overlap seen in the Western North Pacific (Fig. S2). These results help quantify the sensitivity of ET location to various methodological choices, and the results presented in Fig. 16 are necessarily sensitive to such choices, as are other published analyses. The method should fit the research question. When ET completion is identified post-warm core, it is broadly co-located with climatological, basin-high values of Eady growth rate (Fig. S2), indicating that this approach may be preferable for analyses of ET location, particularly in the North Atlantic.

In addition, application to climate models presents additional concerns. Bieli et al. (2020) identified grid-scale convective updrafts in 50-km-resolution simulations with the Forecast-oriented Low Ocean Resolution (FLOR) version of the GFDL CM2.5 that triggered erroneous diagnoses of warm- and cold-core cyclone structures. These were rectified by computing storm-centric 95th-percentile geopotential (rather than local maxima) and by applying a temporal smoothing to phase-space trajectories. Although these issues are not pertinent to all models, understanding the effect of convection-parameterisation schemes on geopotential maxima and phase-space results, particularly T_U , requires a systematic investigation across

multiple high-resolution models, contrasting simulations run using parameterised versus explicitly resolved convection.

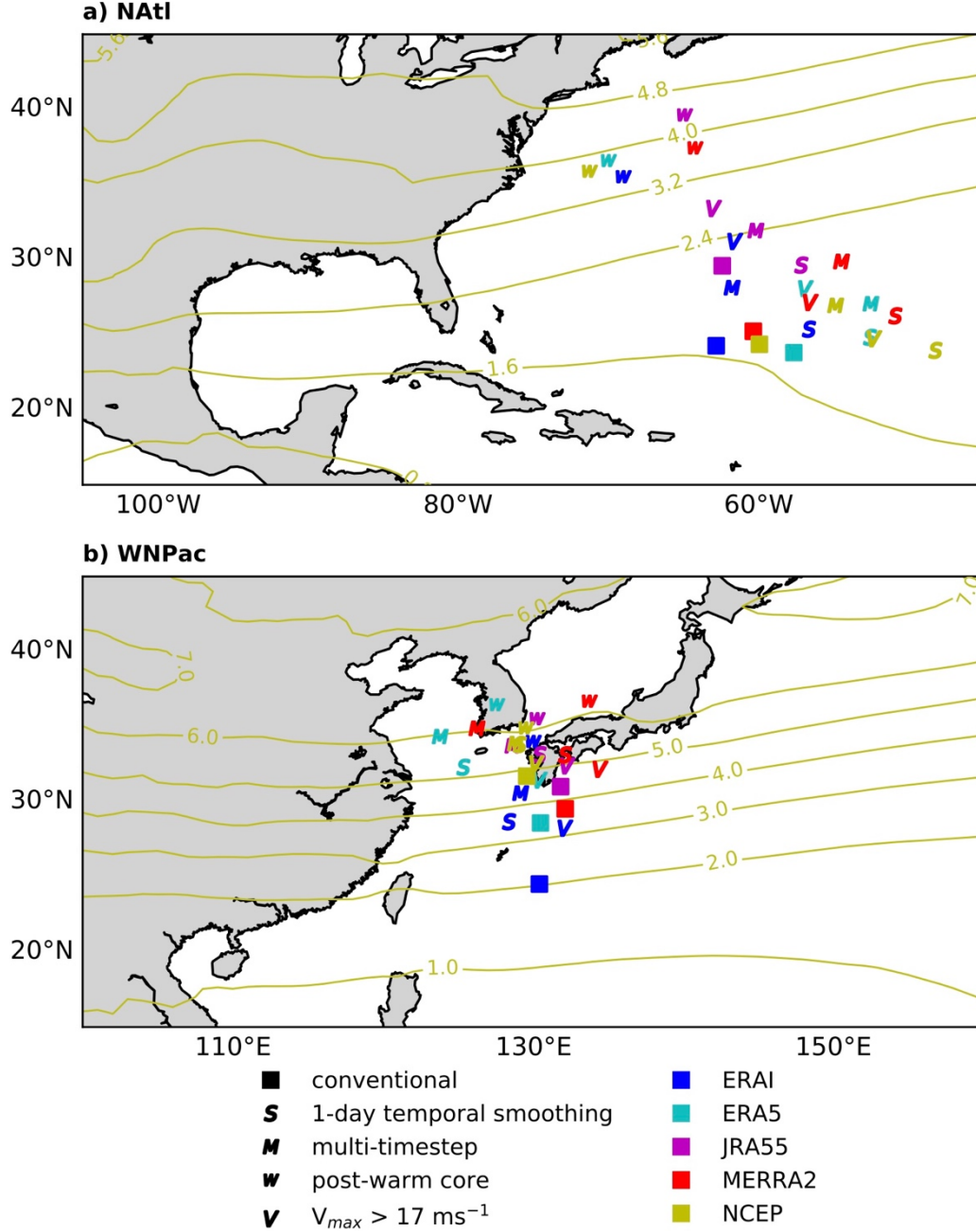


Fig. S2. Sensitivity of ET-completion location in reanalyses to published methodological approaches. Results are shown for (a) the North Atlantic ('NAtl') and (b) the Western North Pacific ('WNPac'). 'Conventional' (square markers) refers to the commonly used definition of ET completion: the first timestep at which both B and T_L indicate an extratropical structure. The other markers indicate a single modification of this definition. 'S': a 24-hour temporal smoothing of B and T_L trajectories was applied. 'M': ET completion is only identified where B and T_L criteria are satisfied for four consecutive timesteps. 'V': ET completion is only

identified for storms whose lifetime-maximum intensity exceeds 17 ms^{-1} . ‘WC’: a warm core lasting for at least two days is first identified for each storm and ET completion is identified thereafter. Overlain are contours of climatological-mean Eady growth rate maxima for August–November in units of day^{-1} , computed using ERA5 wind and geopotential data using Eq. 4.

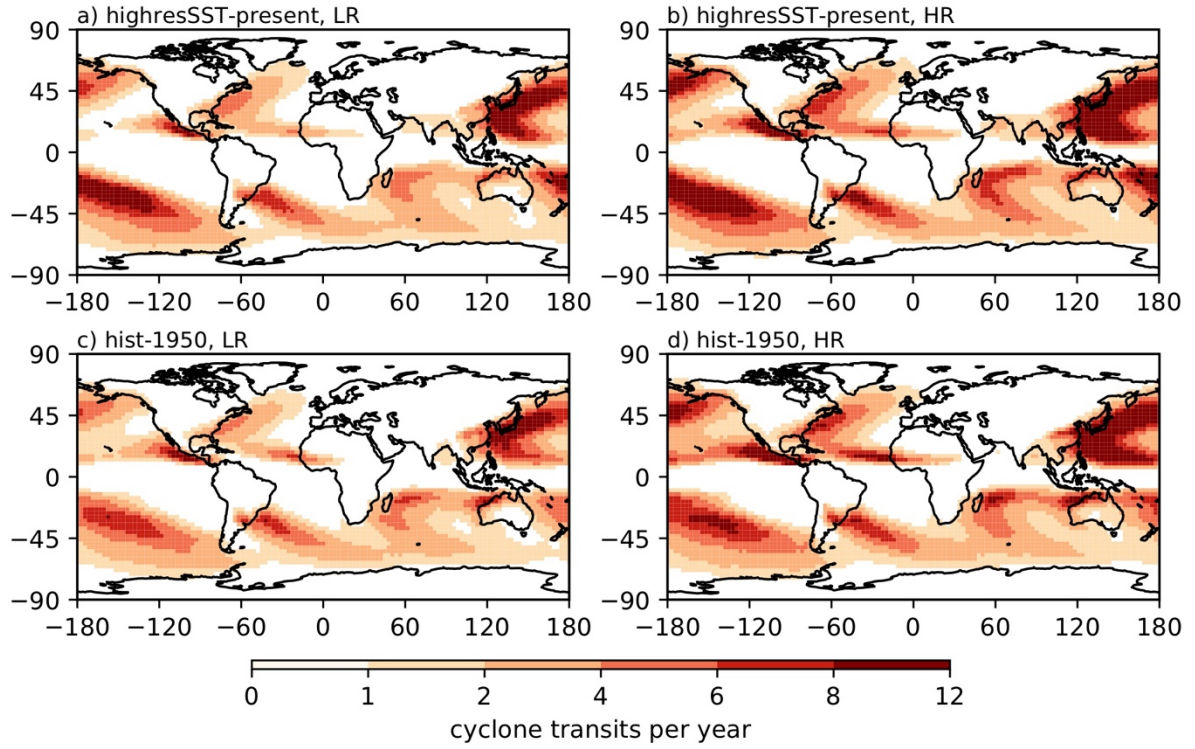


Fig. S3. Historical ensemble-mean track density simulated in low- and high-resolution (a–b) *highresSST-present* and (c–d) *hist-1950* experiments. Unit is cyclone transits per year per unit area (within a 5° geodesic radius of storm centres). Colour scale is the same as in Fig. 1a.

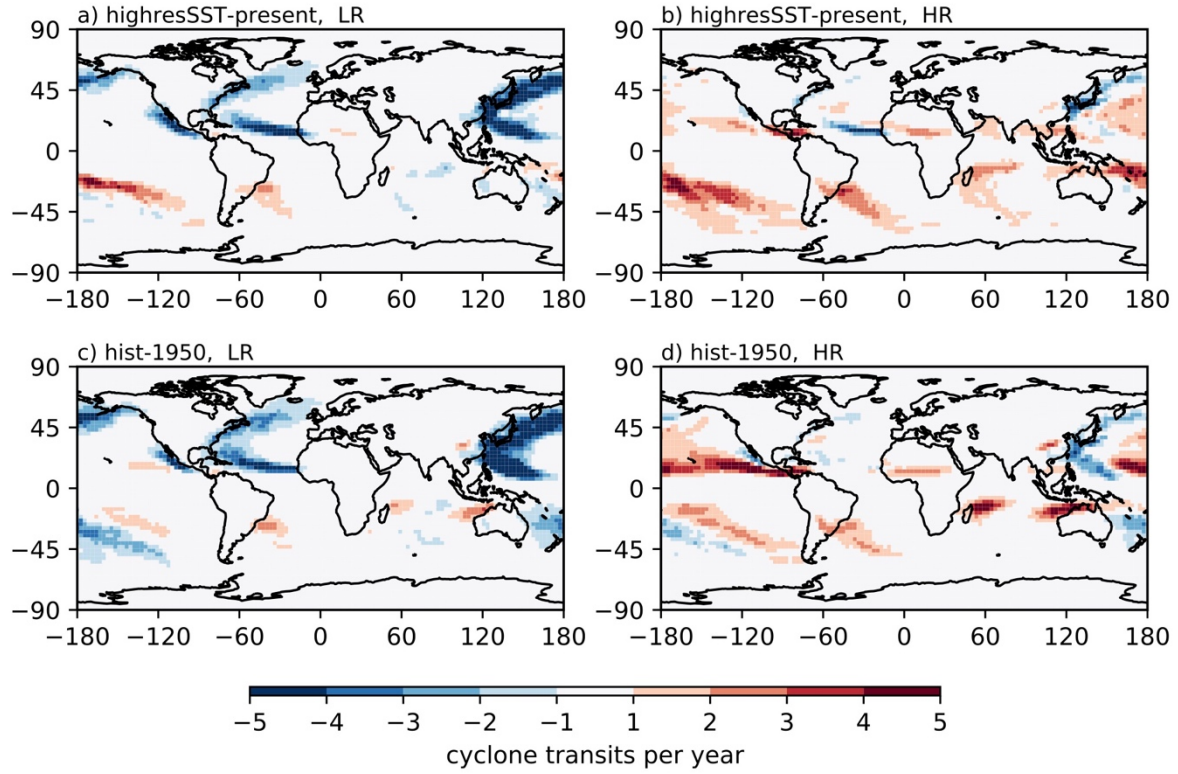


Fig. S4. Historical ensemble-mean track density biases (compared with multireanalysis-mean track density) simulated in low- and high-resolution (a–b) *highresSST-present* and (c–d) *hist-1950* experiments. Unit is cyclone transits per year per unit area (within a 5° geodesic radius of storm centres). Colour scale is the same as in Fig. 1c, e.

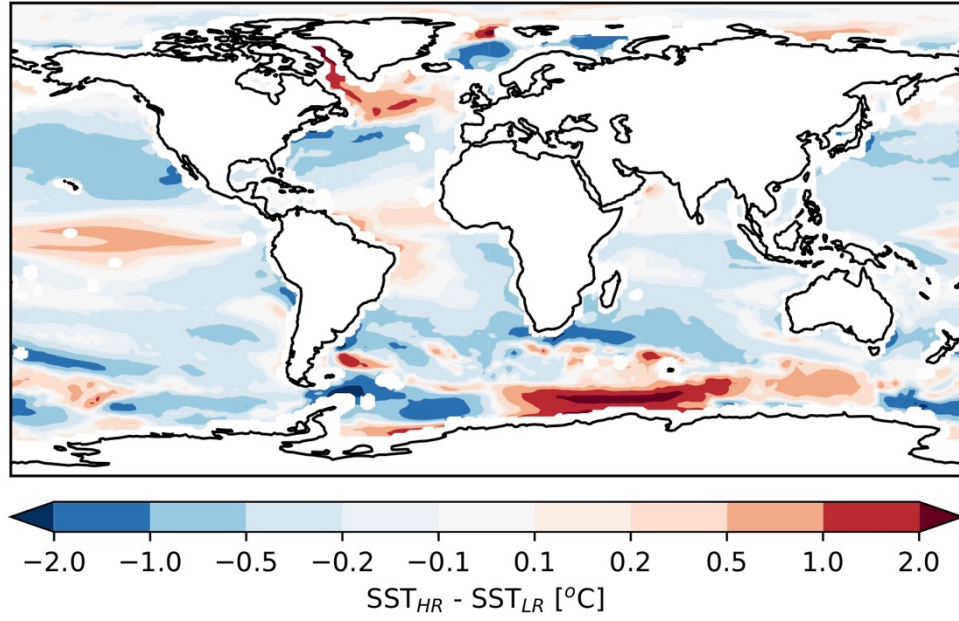


Fig. S5. Historical ensemble-mean August-November SST difference between low- and high-resolution *hist-1950* simulations. The low- and high-resolution sub-ensembles correspond to those of Fig. 1. Note the non-linear colour scale.

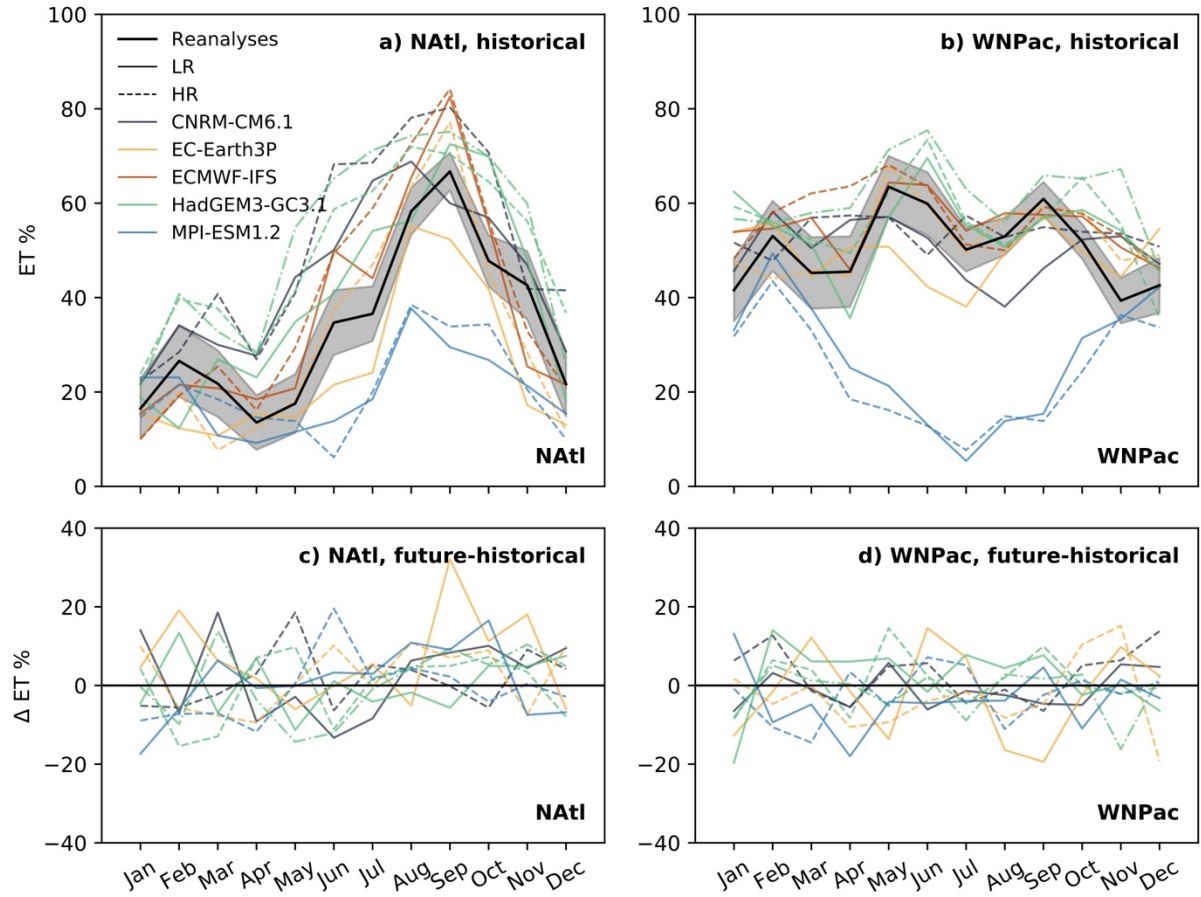


Fig. S6. Historical seasonal cycle of ET % in the (a) North Atlantic and (b) Western North Pacific basins. Shown are the multireanalysis mean (black with shading indicating standard error) and low- (solid) and high-resolution (dashed) *highresSST-present* simulations. (c–d) The difference between the future and historical seasonal cycles in ET % (i.e., *highresSST-future* minus *highresSST-present*). HadGEM3-GC3.1-MM is indicated by the dot-dashed line.

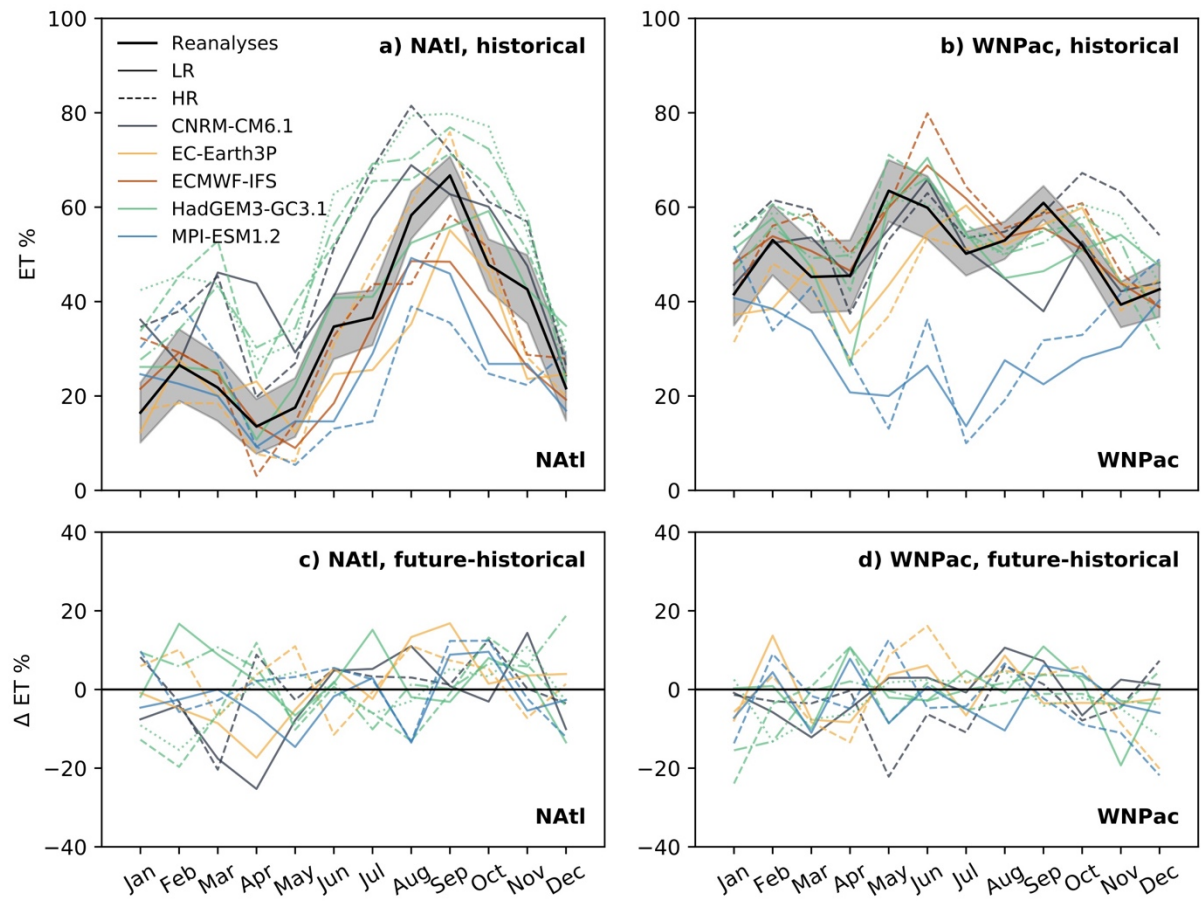


Fig. S7. Same as Fig. S6 but for fully coupled simulations. HadGEM3-GC3.1-MM and -HH are indicated by the dot-dashed and dotted lines, respectively.

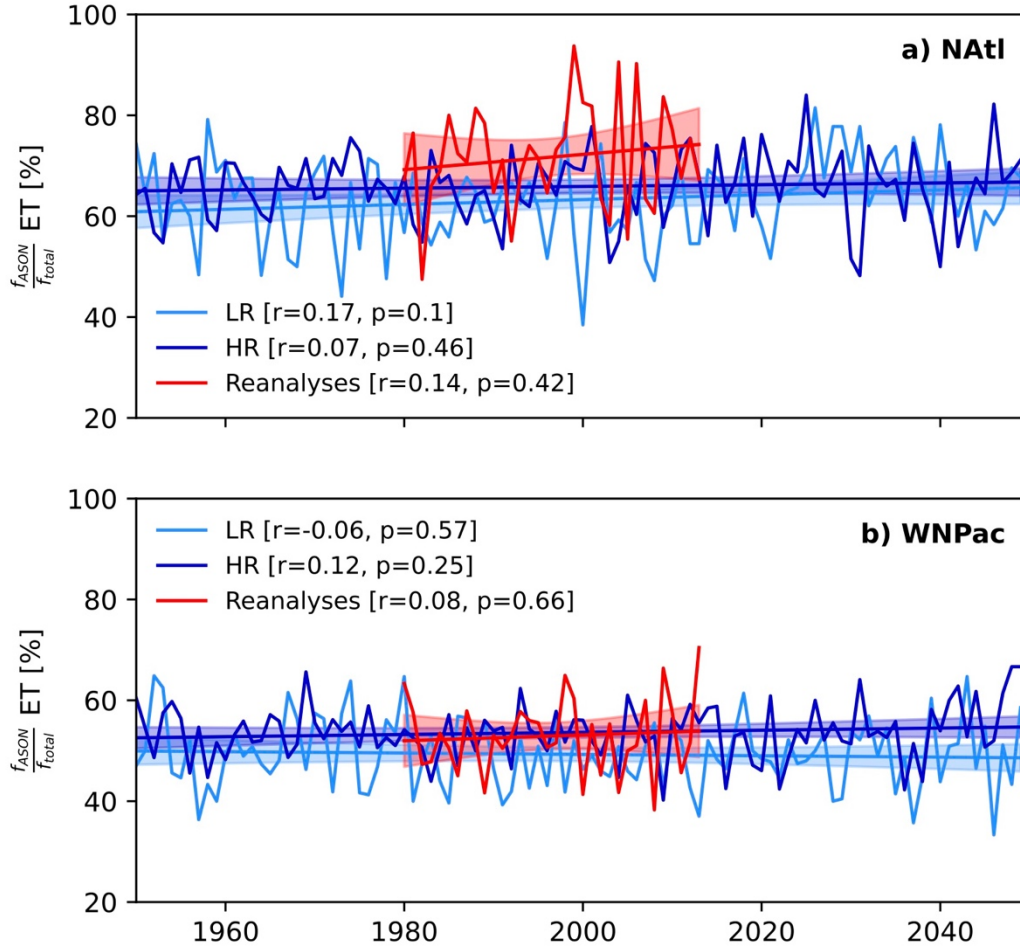


Fig. S8. Secular change in the ensemble-mean proportion of ET events occurring during August–November in reanalyses (red) and in low- (pale blue) and high-resolution (dark blue) fully coupled simulations for (a) the North Atlantic and (b) the Western North Pacific basins. Shading shows the 95 % confidence interval for the linear fit. ECMWF-IFS is not included in this analysis because no future simulations were performed in HighResMIP for this model.